1.0

4.5
50
5.6
6.3

2.8
3.2
3.6
4.0

2.5
2.2
2.0

1.1

1.8

1.25 1.4 1.6

MICROCOPY RESOLUTION TEST CHART
NATIONAL BUREAU OF STANDARDS-1963-A

R78-912864-6

LEVEL

Development of a Viscous Transonic Cascade Analysis

by

J.M. Verdon and M.J. Werle
October, 1978

Final Report for Period 29 April 1977-29 August 1978
Prepared under Contract N00019-77-C-0242

for

Naval Air Systems Command
Department of the Navy
1499 Jefferson Davis Hwy.
Arlington, Va. 22209

by

UNITED TECHNOLOGIES RESEARCH CENTER

UNITED TECHNOLOGIES

EAST HARTFORD, CONNECTICUT 06108

78 11 24 032

78-10-231-1

R78-912864-6

UTRC/R78-912864-6

Development of a Viscous Transonic Cascade Analysis.

by *Michael*

Joseph J.M. Verdon and M.J. Werle

29 October 1978 94 p.

Approved for Public Release; Distribution Unlimited

Final Report for period 29 April 1977-29 August 1978,

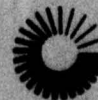Prepared under Contract N00019-77-C-0242

for

Naval Air Systems Command
Department of the Navy
1499 Jefferson Davis Hwy.
Arlington, Va. 22209

by

**UNITED TECHNOLOGIES
RESEARCH CENTER** UNITED TECHNOLOGIES

EAST HARTFORD, CONNECTICUT 06108

78 11 24 032

78-10-231-1

409 252

REPORT DOCUMENTATION PAGE		READ INSTRUCTIONS BEFORE COMPLETING FORM
1. REPORT NUMBER R78-912864-6	2. GOVT ACCESSION NO.	3. RECIPIENT'S CATALOG NUMBER
4. TITLE (and Subtitle) Development of a Viscous Transonic Cascade Analysis		5. TYPE OF REPORT & PERIOD COVERED Final Report April 1977 - August 1978
		6. PERFORMING ORG. REPORT NUMBER UTRC Report R78-912864-6
7. AUTHOR(s) Joseph M. Verdon Michael J. Werle		8. CONTRACT OR GRANT NUMBER(s) N00019-77-C-0242
9. PERFORMING ORGANIZATION NAME AND ADDRESS United Technologies Research Center Silver Lane East Hartford, CT 06108		10. PROGRAM ELEMENT, PROJECT, TASK AREA & WORK UNIT NUMBERS
11. CONTROLLING OFFICE NAME AND ADDRESS		12. REPORT DATE October 29, 1978
		13. NUMBER OF PAGES
14. MONITORING AGENCY NAME & ADDRESS(If different from Controlling Office) Department of the Navy Naval Air Systems Command 1499 Jefferson Davis Hwy Arlington, VA 22209		15. SECURITY CLASS. (of this report) Unclassified
		15a. DECLASSIFICATION/DOWNGRADING SCHEDULE

16. DISTRIBUTION STATEMENT (of this Report)

Approved for Public Release; distribution unlimited.

17. DISTRIBUTION STATEMENT (of the abstract entered in Block 20, if different from Report)

18. SUPPLEMENTARY NOTES

19. KEY WORDS (Continue on reverse side if necessary and identify by block number)

Viscous Flow, Cascade Blade Passage, Navier-Stokes Equations, Alternating Direction, Implicit Time-Marching, Generalized Coordinates, Viscid/Inviscid Interaction, Interacting Boundary Layer, Triple Deck, Trailing Edge

20. ABSTRACT (Continue on reverse side if necessary and identify by block number)

A research program has been conducted towards developing an analysis to predict viscous flow in a cascade blade passage. Two approaches have been investigated. The first concerns obtaining solutions to the compressible Navier-Stokes equations of motion, and the second considers the formulation and numerical solution of viscid/inviscid interaction models for localized flow regions to predict several of the viscous phenomena of importance in turbomachinery applications. In the present effort an existing computer code,

DD FORM 1473 EDITION OF 1 NOV 68 IS OBSOLETE
S/N 0102-LF-014-6601

based on an alternating direction, implicit time-marching solution to a general coordinate representation of the Navier-Stokes equations has been modified to be applicable to the blade passage problem. In addition, a simple external flow field, i.e., flow past a circular cylinder, has been calculated in order to gain experience in working with this code and to assess its reliability and efficiency. In the second part of the present effort an interacting boundary layer model, incorporating asymptotic triple deck concepts, has been constructed to predict the flow in the trailing edge region of an airfoil. Numerical results, based on the triple deck version of this model are presented for both attached and separated laminar super-sonic flows past symmetric sharp trailing edges. Results for a flat plate trailing edge are in good agreement with the previously published numerical results of P. G. Daniels.

ACCESSION for
NTIS
DDC
UNANNOUNCED
JUSTIFICATION

BY
DISTRIBUTION/AVAILABILITY CODES
Dist.   SPECIAL

A

R78-912864-6

Development of a Viscous Transonic Cascade Analysis

TABLE OF CONTENTS

TABLE OF CONTENTS (Cont'd)

INTRODUCTION

An important problem which must be faced by the designer of advanced gas turbine engines is the prediction of the viscous flow field in and around turbine and compressor blade passages. Such a prediction is required to determine heat transfer rates and aerodynamic losses both of which may be critical to successful engine operation. Inaccurate predictions of either loss coefficients or heat transfer rates may result in poor estimates of engine performance or even catastrophic failure of the engine components. For example, excess aerodynamic losses associated with viscous phenomena including boundary layer separations, trailing edge-wake interactions and massive stall may result in a serious deterioration of component efficiency. In addition, excessive heat transfer rates associated with boundary layer separation and reattachment on turbine blades and end walls can have damaging effects as the resulting hot spots may result in structural failure. Since aerodynamic losses and heat transfer rates are associated with the viscous nature of the fluid, the ability to predict the viscous flow field in high performance turbine and compressor blade passages is crucial to the successful design process.

For the flow regimes and configurations of practical interest, in either internal or external aerodynamics, the Reynolds number is usually sufficiently high so that viscous effects are concentrated in relatively thin layers. While this in general allows the direct use of the boundary layer approximation to obtain meaningful predictions of viscous phenomena there are several regions of flow over airfoils where the boundary layer approach breaks down. For example, this approach does not apply in the vicinity of leading edge separations, shock wave/boundary layer interactions, strong blowing sites and trailing edge-wake interactions. The common feature of the flow in these regions is that the boundary layer-like viscous region is displaced from the airfoil surface and exerts a significant influence on the inviscid flow. Therefore it is not surprising that the flow in such regions cannot be adequately described by the usual boundary layer approximation. When viscous displacement effects do alter the inviscid flow field significantly, it is necessary for the calculation procedure to recognize the mutual dependence between the viscous and inviscid regions either by a solution of the full equations of viscous fluid motion throughout the entire region of interest or by a strong interaction analysis between a viscous region solution and an inviscid outer field solution. Thus two methods of approach are currently available which offer the long term prospect of providing useful viscous aerodynamic design information. One consists of obtaining numerical solutions to the compressible Navier-Stokes equations and the other consists of constructing and numerically solving viscid-inviscid interaction models of localized flow regions.

The emergence of numerical solutions to the Navier-Stokes equations as a viable method for predicting viscous flows is a fairly recent phenomena resulting from rapid advances in numerical analysis coupled with development of high speed computers. Such solutions can be obtained either through solution of the steady-state equations via a relaxaation procedure or through solution of the time-dependent Navier-Stokes equations under the influence of steady boundary conditions. In the latter case, each time-step may be thought of as a step in the relaxation procedure. Time dependent solution procedures may be either explicit or implicit. If the method is explicit, the time-step is governed by stringent stability limits which relate the maximum time-step to the size of the computational grid. If a viscous layer is to be adequately defined, a fine grid is required in the vicinity of the blade surface and in such cases the stability limit would make an explicit calculation impractical. However, implicit methods are not subject to such stability limits, rather they are only limited by the physical time scale of the flow. As a result a time-dependent implicit solution procedure for the three-dimensional Navier-Stokes equations has been developed at UTRC by Briley and McDonald. This computer code is a highly modularized program which has options for two- and three-dimensional modes of operation. In two-dimensions, solutions to a general coordinate representation of the Navier-Stokes equations can be obtained. The code has been used previously to calculate laminar and turbulent flows in ducts and low to moderate Reynolds number flows past simple aerodynamic shapes, and it could form a basis for the calculation of viscous flows through cascades. Such solutions would include viscous effects and would be extendable to turbulent flows and to three-dimensional and time-dependent problems. It is anticipated, however, that the computing time required to obtain Navier-Stokes solutions for cascade flows may limit the usefulness of such solutions to the turbomachinery designer. In addition, there is some doubt at present that stable Navier-Stokes solutions can be obtained in the Reynolds number range of practical interest (i.e., $Re = O(10^6)$). Future research should do much to alleviate these limitations but at this juncture the prospect of effectively using Navier-Stokes calculations for design applications still seem to be far off.

Although the Navier-Stokes equations contain all the necessary physics to describe viscous separation phenomena, it has long been felt that an intermediate theoretical approach, i.e., a viscous/inviscid interaction model could provide a useful basis for describing a large class of boundary layer departure flows. The results of relatively recent numerical experiments do provide empirical support for the use of such models for both low and high speed flows. In those cases where detailed investigations have been conducted, predictions based on viscous/inviscid interaction models have been found to reproduce Navier-Stokes predictions and/or experimental data at moderate to high Reynolds numbers.

Viscid-inviscid interaction models (interaction boundary layer, triple deck, etc.) consider three basic elements of the flow: an inviscid region, a viscous region which is shear layer like and an interaction region which actively connects the two. Such a model allows one to focus attention on the significant phenomena in their respective flow regions and therefore develop efficient and reliable solution techniques tailored to the needs of each individual region. Numerous examples exist where the interacting boundary layer concept has been successfully applied to laminar and turbulent separation bubbles in external aerodynamics problems. In addition, the triple deck equations, which are a subset of the interacting boundary layer equations, have been used to rigorously study and solve trailing edge flows. Much fundamental work has been done for laminar flow past sharp and blunt (unstalled) trailing edges and Melnik, Chow and Mead have achieved a dramatic success for at least one highly important practical problem, the prediction of Reynolds number effects on the lift (Kutta condition) for turbulent flow past transonic airfoils with sharp, attached flow, trailing edges. Finally, recent fundamental work indicates that the combination of classical free streamline theory and viscid-inviscid interaction concepts will provide a valid model for predicting the major features of massive stall phenomena.

It currently appears that viscid-inviscid interaction models have the potential of providing fast and accurate predictions of several of the viscous phenomena of importance in turbomachinery applications. As such, interaction concepts appear to hold the promise of producing useful and efficient design calculation procedures for turbomachinery applications. Since the interaction equations are a subset of the Navier-Stokes equations and as such identify the dominant terms in those equations and the appropriate scaling laws and correlation parameters, then development of numerical techniques for viscid-inviscid interaction models may have a direct impact on, and indeed may be a prerequisite for the development of reliable and efficient ways to solve the Navier-Stokes equations in the high Reynolds number regime.

With the foregoing considerations in mind a research effort has been conducted to develop an analysis for the prediction of high Reynolds number flow in a cascade passage. Under the present study an existing implicit time-marching Navier-Stokes computer code has been further developed to treat cascade flows. In particular, the general coefficient, matrix inversion, and boundary condition subroutines have been modified to allow for the specification of cascade blade-to-blade periodicity conditions. In addition, calculations have been performed to assess the reliability and accuracy of the Navier-Stokes computer code and to verify the successful completion of the coding changes made under the present contract. Finally, an effort has been initiated towards bringing viscous/inviscid interaction concepts to bear on the viscous phenomena of importance in turbomachinery flows. In particular,

3

a viscous/inviscid interaction model incorporating asymptotic triple deck concepts has been formulated for high Reynolds number laminar trailing edge flows. Numerical solution procedures based on the triple deck version of this model have been developed and results for both attached and separated "stalled" trailing edge flows have been obtained.

PART I

DEVELOPMENT OF A NAVIER-STOKES SOLUTION PROCEDURE

FOR VISCOUS CASCADE FLOWS

LIST OF SYMBOLS - PART I

Except where dimensions are specified, all quantities in the following are nondimensional; physical velocities are normalized by U_r, density by ρ_r, pressure by $\rho_r U_r^2$, dynamic viscosity by μ_r, and time by L_r/U_r where L_r is the reference length.

$a_{i,j,k}^n$	Coefficient matrix, Eq. (I-21)
A	Constant defined in Eq. (I-3) Coefficient matrix, Eq. (I-15a)
$b_{i,j,k}^n$	Coefficient matrix, Eq. (I-21)
B	Constant, defined in Eq. (I-3)
$c_{i,j,k}^n$	Coefficient matrix, Eq. (I-21)
$d_{i,j,k}^n$	Column vector, Eq. (I-21)
D_m, D_m^2	Finite difference operators for coordinate y^m
D_{ij}^{km}	Momentum equation coefficient, Eq. (I-6)
D_r, D_θ	Damping constants for coordinate transformations, Eqs. (I-24)
$\mathcal{D}$	Column vector function of the dependent variables and their spatial derivatives in a single coordinate direction, Eq. (I-9)
$\mathcal{D}_{BC}$	Boundary condition matrix operator, Eq. (I-30)
$\mathcal{D}_m$	Column vector containing spatial derivatives of the dependent variables in the y^m - direction only, Eq. (I-17)
$\vec{e}_{(i)}$	Coordinate base vector, Eqs. (I-35)
E_{ij}^k	Momentum equation coefficient, Eq. (I-7)
F_{ijk}^m	Momentum equation coefficient, Eq. (I-6)
g_{ij}	Metric tensor coefficient
g^{ij}	Inverse metric tensor coefficient

G_{ijk} Momentum equation coefficient, Eq. (I-6)

H Column vector function of the dependent variables, Eqs. (I-9, I-10)

I Boundary point index - y^1 - direction

I_{ij} Momentum equation coefficient, Eq. (I-6)

J Jacobian
Boundary point index, y^2 - direction

K Momentum equation coefficient, Eq. (I-6)

L_r Reference length, meters

L_{ij}^k Momentum equation coefficient, Eq. (I-6)

$\mathcal{L}$ Matrix operator, Eq. (I-15c)

$\mathcal{L}_m$ Matrix operator containing spatial derivatives in the y^m - direction only, Eq. (I-17)

M_r Reference Mach number

$\vec{n}$ Unit outward normal vector

p Pressure

r Computational radial coordinate

R Physical radial coordinate

R_i Momentum equation coefficient, Eq. (I-6)

Re Reference Reynolds number, $\rho_r U_r L / \mu_r$

$Re_{\Delta x^m}$ Mesh Reynolds number, $|U_m| \Delta x^m Re$

S Column vector containing mixed second order spatial derivative terms, Eq. (I-9)

t Time

T	Temperature
T_o	Total temperature
u_m	Cartesian velocity component, Eq. (I-22)
U_r	Reference speed, meters/sec
$\vec{v}$	Velocity vector
v^i	Contravariant velocity component
$v(i)$	Physical velocity component
y^i	Computational curvilinear coordinate
α	Spatial differencing parameter, Eq. (I-20)
β, β_1, β_2	Temporal differencing parameters, Eqs. (I-11, I-12)
γ	Specific heat rates, c_p/c_v
δ_i^j	Kronecker delta
Δt	Time increment
Δx^m	Mesh spacing for cartesian coordinate x^m, Eq. (I-22)
Δy^m	Mesh spacing for coordinate y^m
$\Delta r, \Delta \theta$	Mesh spacing for computational polar coordinates r and θ
Δ_+, Δ_-	Spatial difference operators, Eq. (I-20)
ϵ	Convergence parameter, Eq. (I-34)
ϵ_m	Artificial viscosity, Eq. (I-22)
θ, θ	Angular polar computational and physical coordinates

μ   Dynamic viscosity

ρ   Density

φ   Dependent variable column vector, Eq. (I-9)

ψ   Dependent variable column vector, Eq. (I-15a)

ω   Fourth derivation dissipation coefficient, Eq. (I-23)

Subscripts

i,j,k Denote covariant tensor components or function evaluated at grid point (y^i, y^j, y^k)

r   Denotes dimensional reference value

$t=0$ Denotes inviscid initial solution

$,i$ Denotes covariant derivative with respect to coordinate y^i

Superscripts

i,j,k Denote contravariant tensor component or grid point location

L   Denotes lower periodic boundary of blade passage

U   Denotes upper periodic boundary of blade passage

*, **   Denote intermediate solutions of alternating direction procedure

BACKGROUND

The UTRC Navier-Stokes computer code obtains implicit time-marching finite difference solutions to a general coordinate representation of the equations of motion. The numerical solution procedure on which this code is based was originally developed by Briley and McDonald (Ref. I-1). A typical time step in their procedure consists of a time-wise linearization followed by a fully implicit difference approximation which is solved by an ADI (Alternating Direction Implicit) procedure of the Douglas-Gunn type (Ref. I-2). The advantage with ADI methods is that a short sequence of simple matrix inversions replaces the complicated matrix inversion problem associated with a direct solution of the implicit equations. In this way a real savings in computer time is made without sacrificing accuracy or stability. Briley, McDonald, and Gibeling (Ref. I-3) have shown that the ADI scheme has run stably and accurately with time steps which are orders of magnitude larger than the explicit stability limit (Ref. I-4). The first applications of the implicit time-marching Navier-Stokes computer code involved the calculation of laminar and turbulent flows in rectangular ducts (Refs. I-1 and I-3). Recently the basic numerical analysis (and computer code) has been extended by Gibeling, Shamroth and Eiseman to consider a general curvilinear coordinate form of the Navier-Stokes equations. In addition, they applied the curvilinear coordinate version of the Navier-Stokes code to calculate low to moderate Reynolds number external flows past simple aerodynamic shapes (Ref. I-5).

In the present effort sample external flow calculations have been performed to assess the reliability and accuracy of the current version of the implicit time-marching Navier-Stokes computer code, and this code has been modified to treat cascade blade passage flows. The governing equations and numerical solution procedure upon which the UTRC Navier-Stokes computer code is based will be outlined below for the special case of laminar, steady adiabatic flow. The equations of motion and the numerical solution procedure are described for three-dimensional flows; however, only two-dimensional applications have been considered herein. For a more general treatment of the governing equations and more complete details on the numerical method the reader is referred to References I-1, I-3, and I-5.

EQUATIONS OF MOTION

All quantities in the following equations are dimensionless; physical velocities are normalized by U_r, density by ρ_r, pressure by $\rho_r U^2_r$, temperature by T_r, molecular viscosity by μ_r, length by L_r, and time by U_r/L_r. The fluid is assumed to be a perfect gas with zero bulk viscosity coefficient and constant molecular viscosity and specific heat. The flow is assumed to be adiabatic with constant total temperature, T_o, and body forces are assumed to be negligible. Under these assumptions, the Navier-Stokes equations can be written for time-independent, curvilinear coordinates (y^1, y^2, y^3) as follows (Ref. I-6): the continuity equation is

$$\frac{\partial \rho}{\partial t} + (\rho v^i)_{,i} = 0 \tag{I-1}$$

and the momentum equations are given by

$$\rho \left(\frac{\partial v^i}{\partial t} + v^j v^i_{,j} \right) = -g^{ij} p_{,j} + \frac{\mu}{3Re} g^{ij} v^k_{,kj} + \frac{\mu g^{jk}}{Re} v^i_{,jk} \tag{I-2}$$

where ρ is the density, $\vec{v}$ is the velocity, p is the pressure, μ is the molecular viscosity, $Re = \rho_r U_r L_r/\mu_r$ is the Reynolds number. In addition, g^{ij} are components of the inverse metric, v^i are contravariant velocity components, subscripts after commas denote covariant derivatives, the indices i, j, and k vary from 1 to 3, and repeated indices are to be summed. The energy equation can be replaced with an adiabatic equation of state

$$p = \rho \left[A + B g_{ij} v^i v^j \right] \tag{I-3}$$

where $A = T_o/\gamma M_r^2$, $B = (\gamma - 1)/2\gamma$, g_{ij} are components of the metric tensor, M_r is the reference Mach number, and γ is the specific heat ratio (c_p/c_v).

After substituting Eq. (I-3) into Eq. (I-2) to eliminate the pressure, the governing equations can be expressed in a convenient form for numerical calculations (Ref. I-5). It follows after some algebra that

$$\frac{\partial (\rho J)}{\partial t} + \frac{\partial}{\partial y^j} (\rho J v^j) = 0 \tag{I-4}$$

11

and

$$\frac{\partial}{\partial t}\left(Jg_{ij}\rho v^j\right) + K\frac{\partial \rho}{\partial y^i} + F_{jki}^m \frac{\partial}{\partial y^m}\left(\rho v^j v^k\right)$$

$$+ L_{ij}^k \frac{\partial v^j}{\partial y^k} + D_{ij}^{km} \frac{\partial^2 v^j}{\partial y^k \partial y^m} + R_i \rho + I_{ij} v^j$$ (I-5)

$$+ G_{ijk}\, \rho v^j v^k = 0$$

The coefficients in Eq. (I-5) are defined by

$$K = AJ$$

$$F_{jki}^m = \left(g_{ij}\,\delta_k^m + Bg_{jk}\,\delta_i^m\right)J$$

$$G_{ijk} = \frac{\partial F_{jki}^m}{\partial y^m} - \frac{J}{2}\frac{\partial g_{mn}}{\partial y^i}\left(\delta_j^m\,\delta_k^n + Bg_{jk}\,g^{mn}\right)$$

$$R_i = A\frac{\partial J}{\partial y^j}\,\delta_i^j - \frac{J}{2}\,A\,\frac{\partial g_{jk}}{\partial y^i}\,g^{jk}$$ (I-6)

$$D_{ij}^{km} = \frac{\mu}{Re}\,J\left[\frac{2}{3}\,\delta_i^k\,\delta_j^m - g_{ij}g^{km} - \delta_j^k\,\delta_i^m\right]$$

$$I_{ij} = \frac{\partial E_{ij}^k}{\partial y^k} + \frac{\mu}{2Re}\,\frac{\partial g_{mk}}{\partial y^i}\left[Jg^{nm}\,g^{pk}\,\frac{\partial g_{pn}}{\partial y^j} - \frac{2}{3}\,\frac{\partial J}{\partial y^j}\,g^{mk}\right]$$

$$L_{ij}^k = E_{ij}^k + \frac{\partial D_{ij}^{mk}}{\partial y^m} + \frac{\mu}{2Re}\,J\,\frac{\partial g_{nm}}{\partial y^i}\left[g^{kn}\,\delta_j^m + g^{km}\,\delta_j^n - \frac{2}{3}\,g^{nm}\,\delta_j^k\right]$$

where the Kronecker symbol δ_i^j vanishes unless $i = j$ in which case it is unity and

$$E_{ij}^k = \frac{\mu}{Re}\left[\frac{2}{3}\,\frac{\partial J}{\partial y^j}\,\delta_i^k - Jg^{mk}\,\frac{\partial g_{im}}{\partial y^j}\right]$$ (I-7)

Equations (I-4) and (I-5) are the Navier-Stokes equations in a fixed coordinate frame (y^1, y^2, y^3) with the density, ρ, and the contravariant velocity components, v^i, $i = 1, 2, 3$, taken as dependent variables. Once the curvilinear coordinate system is prescribed, the Jacobian and metric tensor components and hence the coefficients, defined by Eqs. (I-6) and (I-7), become known

12

functions of the spatial coordinates. Previous experience (Ref. I-5) has indicated that the use of contravariant velocity components as dependent variables can lead to serious truncation errors and as a result the current version of the UTRC Navier-Stokes computer code has been formulated to consider the density and the physical velocity components, v(i) as basic dependent variables, where

$$v(i) = (g_{ii})^{1/2} \, v^i \qquad \text{(no sum on i)} \qquad (I-8)$$

The appropriate form of the Navier-Stokes equations is then obtained after substituting Eq. (I-8) into Eqs. (I-4) and (I-5).

Although the use of generalized (nonorthogonal) coordinates leads to a complicated form of the equations of motion. Such coordinates offer significant computational advantages. In particular, physical boundaries of the flow region can be represented as coordinate surfaces, thus removing the need for fractional cells and boundary condition interpolations. Further, a uniform mesh can be used in computational space and mapped into a mesh suitably distributed in physical space to capture large solution gradients such as those occurring in boudary layers and near airfoil leading and trailing edges. Finally, the uniform mesh in computational space simplifies the finite difference approximations of derivative terms.

NUMERICAL SOLUTION PROCEDURE

The numerical method can be briefly outlined as follows: the governing equations are replaced by an implicit time difference approximation, optionally a backward difference or Crank-Nicolson scheme. Terms involving nonlinearities at the implicit time level are linearized by Taylor expansion about the solution at the known time level, and spatial difference approximations are introduced. The result is a system of linear difference equations for the dependent variables at the unknown or implicit time level. To solve these difference equations, the Douglas-Gunn (Ref. I-2) procedure for generating alternating-direction implicit (ADI) schemes is introduced. This technique leads to systems of coupled linear difference equations having narrow block-banded matrix structures which can be solved efficiently by standard block-elimination methods.

To describe the numerical procedure it is convenient to express the Navier-Stokes equations in the following matrix form:

$$\frac{\partial H(\phi)}{\partial t} = \mathcal{D}(\phi) + S(\phi) \tag{I-9}$$

where ϕ is a column vector containing the dependent variables, H is a column vector function of ϕ, $\mathcal{D}$ is a column vector whose elements are functions of the dependent variables and their spatial derivatives in a single coordinate direction, and S is a column vector whose elements are functions of the mixed second order spatial derivatives of the dependent variables. For example, when the contravariant velocity components are treated as dependent variables, ϕ, H (ϕ) and S (ϕ) have the form (cf. Eqs. (I-4) and (I-5)):

$$\phi = \begin{bmatrix} \rho \\ v^1 \\ v^2 \\ v^3 \end{bmatrix} \qquad\qquad H = \begin{bmatrix} J\rho \\ Jg_{ij}\rho v^j \\ Jg_{2j}\rho v^j \\ Jg_{3j}\rho v^j \end{bmatrix}$$

$$\tag{I-10}$$

$$S = \begin{bmatrix} \left(D_{1j}^{12} + D_{1j}^{21}\right)\dfrac{\partial^2 v^j}{\partial y^1 \partial y^2} + \left(D_{1j}^{13} + D_{1j}^{31}\right)\dfrac{\partial^2 v^j}{\partial y^1 \partial y^3} + \left(D_{1j}^{23} + D_{1j}^{32}\right)\dfrac{\partial^2 v^j}{\partial y^2 \partial y^3} \\[2ex] \left(D_{2j}^{12} + D_{2j}^{21}\right)\dfrac{\partial^2 v^j}{\partial y^1 \partial y^2} + \left(D_{2j}^{13} + D_{2j}^{31}\right)\dfrac{\partial^2 v^j}{\partial y^1 \partial y^3} + \left(D_{2j}^{23} + D_{2j}^{32}\right)\dfrac{\partial^2 v^j}{\partial y^2 \partial y^3} \\[2ex] \left(D_{3j}^{12} + D_{3j}^{21}\right)\dfrac{\partial^2 v^j}{\partial y^1 \partial y^2} + \left(D_{3j}^{13} + D_{3j}^{31}\right)\dfrac{\partial^2 v^j}{\partial y^1 \partial y^3} + \left(D_{3j}^{23} + D_{3j}^{32}\right)\dfrac{\partial^2 v^j}{\partial y^2 \partial y^3} \end{bmatrix}$$

and the elements of the column vector $\mathcal{D}(\phi)$ consist of the remaining terms in Eqs. (I-4) and (I-5). It should be noted, that certain definitions and descriptions of terms provided in the present discussion differ from those given earlier in Refs. I-1, I-3 and I-5. However, the definitions used here are appropriate to the current version of the implicit time-marching Navier-Stokes computer code.

The solution domain is discretized by grid points having equal spacings in the computational coordinates, Δy^1, Δy^2, and Δy^3 in the y^1, y^2 and y^3 directions, respectively, and an arbitrary time step, Δt. The subscripts i, j, k and superscript n are grid point indices associated with y^1, y^2, y^3 and t, respectively, and thus $\phi^n_{i,j,k}$ denotes $\phi(y^1_i, y^2_j, y^3_k, t^n)$. It is assumed that the solution is known at the n level, t^n, and is desired at the (n + 1) level, t^{n+1}. At the risk of an occasional ambiguity, one or more of the subscripts is frequently omitted, so that ϕ^n is equivalent to $\phi^n_{i,j,k}$.

Linearization Scheme

A linear difference approximation to the nonlinear governing equations is obtained from the following time-difference replacement of Eq. (I-9):

$$\left(H^{n+1} - H^n\right)/\Delta t = \beta_1 \, \mathcal{D}^{n+1} + (1-\beta_1)\, \mathcal{D}^n + \beta_2 \, S^{n+1} + (1-\beta_2)\, S^n \tag{I-11}$$

where, for example, $H^{n+1} = H(\phi^{n+1})$. The parameters $(0 \leq \beta_1, \beta_2 \leq 1)$ permit variable centering of the scheme in time. Thus Eq. (I-11) produces a backward difference or fully implicit formulation for $\beta_1 = \beta_2 = 1$, a Crank-Nicolson formulation for $\beta_1 = \beta_2 = 1/2$, and a forward difference or fully explicit scheme for $\beta_1 = \beta_2 = 0$. Unconditional stability is anticipated for $\beta_1, \beta_2 > 1/2$. In the present method the column vector $S(\phi)$ is treated explicitly. Thus with $\beta = \beta_1$, Eq. (I-11) reduces to

$$\left(H^{n+1} - H^n\right)/\Delta t = \beta_1 \, \mathcal{D}^{n+1} + (1-\beta)\, \mathcal{D}^n + S^n \tag{I-12}$$

The mixed derivative terms (in $S(\phi)$) could be treated implicitly within the ADI framework; however, this would increase the number of intermediate steps and thereby complicate the solution procedure. Test cases computed while developing the present numerical method (Refs. I-1 and I-3) have indicated that the explicit treatment of mixed derivative terms has no observable adverse affect on stability.

The linearization is accomplished by a two step process of expansion about the known time level t^n and subsequent approximation of the quantity $(\partial\phi/\partial t)^n \Delta t$, which arises from chain rule differentiation, by $(\phi^{n+1} - \phi^n)$. The result is

$$H^{n+1} = H^n + (\partial H/\partial\phi)^n (\phi^{n+1} - \phi^n) + \mathcal{O}(\Delta t)^2 \qquad (\text{I-13a})$$

$$\mathcal{D}^{n+1} = \mathcal{D}^n + (\partial\mathcal{D}/\partial\phi)^n (\phi^{n+1} - \phi^n) + \mathcal{O}(\Delta t)^2 \qquad (\text{I-13b})$$

The matrix $\partial H/\partial\phi$ is a standard Jacobian whose elements are defined by $(\partial H/\partial\phi)_{qr} \equiv \partial H_q/\partial\phi_r$. The operator elements of the matrix $\partial\mathcal{D}/\partial\phi$ are similarly ordered, i.e., $(\partial\mathcal{D}/\partial\phi)_{qr} = \partial\mathcal{D}_q/\partial\phi_r$ however, the intended meaning of the operator elements requires some clarification. For the qth row, the operation $(\partial\mathcal{D}_q/\partial\phi)^n (\phi^{n+1} - \phi^n)$ is understood to mean that $\{\partial/\partial t \ \mathcal{D}_q [\phi(y^1, y^2, y^3, t)]\}^n \Delta t$ is computed and that all occurrences of $(\partial\phi_r/\partial t)^n$ arising from chain rule differentiation are replaced by $(\phi_r^{n+1} - \phi_r^n)/\Delta t$. The substitution of Eqs. (I-13) into Eq. (I-12) leads to the following linear, implicit, first order accurate time-differenced scheme:

$$\left(\frac{\partial H}{\partial\phi}\right)^n (\phi^{n+1} - \phi^n)/\Delta t = \beta\left(\frac{\partial\mathcal{D}}{\partial\phi}\right)^n (\phi^{n+1} - \phi^n) + \mathcal{D}^n + S^n \qquad (\text{I-14})$$

Equation (I-14) is linear in the quantity $(\phi^{n+1} - \phi^n)$ and all other quantities are either known or evaluated at the nth time level. It is convenient to solve Eq. (I-14) for $(\phi^{n+1} - \phi^n)$ rather than ϕ^{n+1}. This reduces roundoff errors, since it is presumably better to compute a small $0(\Delta t)$ change in an $0(1)$ quantity than the quantity itself. After defining the symbols:

$$\psi \equiv \phi - \phi^n \qquad (\text{I-15a})$$

$$A \equiv \left(\frac{\partial H}{\partial\phi}\right)^n \qquad (\text{I-15b})$$

$$\mathcal{L} \equiv -\beta (\partial\mathcal{D}/\partial\phi)^n \qquad (\text{I-15c})$$

Equations (I-14) can be written in the following simplified form

$$(A + \Delta t \mathcal{L}) \psi^{n+1} = \Delta t [\mathcal{D}^n + S^n] \qquad (\text{I-16})$$

Alternating Direction Procedure

The solution of Eq. (I-16) is accomplished by application of an alter-
nating-direction implicit (ADI) technique which is a generalization of the
procedure developed by Douglas and Gunn (Ref. I-2) for generating ADI schemes
as perturbations of fundamental implicit difference schemes such as the back-
ward-differences or Crank-Nicolson schemes. The vector operator $\mathcal{D}(\phi)$ contains
terms which are functions of ϕ and, in addition, terms which are functions of
ϕ and the first and second order derivatives of ϕ with respect to y^1, y^2, and
y^3, but no mixed derivatives. Thus $\mathcal{D}$ (and hence $\mathcal{L}$) can be split into three
operators, $\mathcal{D}_1, \mathcal{D}_2, \mathcal{D}_3$, associated with the y^1, y^2, and y^3 coordinates, each
having the functional form $\mathcal{D}_m = \mathcal{F}(\phi, \partial/\partial y^m, \partial^2/\partial y^m \partial y^m)$. Those terms of
$\mathcal{D}(\phi)$ which do not contain a spatial derivative are grouped under the operator
$\mathcal{D}_1$. Equation (I-16) then becomes

$$\left[A + \Delta t \left(\mathcal{L}_1 + \mathcal{L}_2 + \mathcal{L}_3 \right) \right] \psi^{n+1} = \Delta t \left[\mathcal{D}_1^n + \mathcal{D}_2^n + \mathcal{D}_3^n + S_n \right] \tag{I-17}$$

and the Douglas-Gunn representation of Eq. (I-17) can be written as the fol-
lowing three step solution procedure:

$$\left(A + \Delta t \, \mathcal{L}_1 \right) \psi^* = \Delta t \left[\mathcal{D}_1^n + \mathcal{D}_2^n + \mathcal{D}_3^n + S^n \right] \tag{I-18a}$$

$$\left(A + \Delta t \, \mathcal{L}_2 \right) \psi^{**} = A \psi^* \tag{I-18b}$$

$$\left(A + \Delta t \, \mathcal{L}_3 \right) \psi^{n+1} = A \psi^{**} \tag{I-18c}$$

where ψ^* and ψ^{**} are intermediate solutions. If ψ^* and ψ^{**} are eliminated,
Eqs. (I-18) become

$$\left(A + \Delta t \, \mathcal{L}_1 \right) A^{-1} \left(A + \Delta t \, \mathcal{L}_2 \right) A^{-1} \left(A + \Delta t \, \mathcal{L}_3 \right) \psi^{n+1} = \Delta t \left[\mathcal{D}_1^n + \mathcal{D}_2^n + \mathcal{D}_3^n + S^n \right] \tag{I-19}$$

and after performing the multiplication on the left-hand side of Eq. (I-19),
it is apparent that Eq. (I-19) approximates Eq. (I-17) to order $(\Delta t)^2$.

Spatial differencing of Eqs. (I-18) is accomplished by replacing deri-
vative operators such as $\partial/\partial y^m$ and $\partial^2/\partial y^m \partial y^m$ (no sum on m) by corresponding
three point finite difference operators, D_m and D_m^2 where

$$D_m \phi \equiv \left[\alpha\Delta_- + (1-\alpha)\Delta_+\right]\phi/\Delta y^m = \partial\phi/\partial y^m + \mathcal{O}\left[(\Delta y)^2 + (\alpha - 1/2)\Delta y^m\right] \quad \text{(I-20a)}$$

$$D_m^2 \phi \equiv (\Delta_+\Delta_-)\phi/\left(\Delta y^m\right)^2 = \partial^2\phi/\partial y^m \partial y^m + \mathcal{O}\left(\Delta y^m\right)^2 \quad \text{(I-20b)}$$

Here, $\Delta_+\phi$ and $\Delta_-\phi$ represent forward and backward differences in ϕ. For example, the difference approximation to the derivative of ϕ at the point (y_i^1, y_j^2, y_k^3) in the y^2 – direction ($m = 2$) is obtained by setting $\Delta_+ \phi_{i,j,k} = \phi_{i,j+1,k} - \phi_{i,j,k}$ and $\Delta_- \phi_{i,j,k} = \phi_{i,j,k} - \phi_{i,j-1,k}$. The parameter α has been introduced ($0 \le \alpha \le 1$) in Eq. (I-20) to permit continuous variation from backward to forward differences. The standard central difference formula is recovered for $\alpha = 1/2$ and was used for the numerical calculations reported here.

With the introduction of the spatial difference operators D_m and D_m^2, defined in Eqs. (I-20), the solution procedure for the alternating direction, implicit time marching form of the governing equations, Eqs. (I-18), can be described. Since D_m and D_m^2 are three point difference operators, the finite difference approximation to Eq. (I-18a) contains $\psi^*_{i-1,j,k}$, $\psi^*_{i,j,k}$, and $\psi^*_{i+1,j,k}$ as unknowns. Hence, the system of linear equations generated by writing Eq. (I-18a) at successive grid points $(y_i^1, y_j^2, y_k^3; i = 1, \ldots, I)$ can be written in block-tridiagonal form; i.e.,

$$a^n_{i,j,k}\psi^*_{i-1,j,k} + b^n_{i,j,k}\psi^*_{i,j,k} + c^n_{i,j,k}\psi^*_{i+1,j,k} = d^n_{i,j,k} \quad \text{(I-21)}$$

where a, b, and c are square matrices and d is a column vector, each containing only n-level quantities. When applied at successive grid points ($i = 1, \ldots, I$), Eq. (21) generates a block-tridiagonal system of equations for ψ^* which, after appropriate treatment of boundary conditions, can be solved efficiently by using standard block-elimination methods (Ref. I-7). The solution procedure for Eqs. (I-18b, c) is analogous to that just described for Eq. (I-18a).

Artificial Dissipation

In computing solutions for high Reynolds number flows, it is often necessary to add a form of artificial viscosity or dissipation. One possible dissipation term in common use is based on an observation by Roache (Ref. I-8) that for a linear model problem representing a one-dimensional balance of convection and diffusion terms, solutions obtained using central differences

for the convection terms are well behaved provided the mesh Reynolds number $Re_{\Delta x^m} = |u_m| \Delta x^m Re$ is ≤ 2, but that qualitative inaccuracies associated with boundary conditions occur for $Re_{\Delta x^m} > 2$. This suggests the use of an artificial viscosity term of the form $\epsilon_m D_m^2 \phi$, where

$$
\epsilon_m = \begin{cases} \dfrac{|u_m| \Delta x^m}{2} - \dfrac{1}{Re} = \dfrac{1}{Re}\left(\dfrac{Re_{\Delta x_m}}{2} - 1\right), \, Re_{\Delta x_m} > 2 \\[4mm] 0 \, , \, Re_{\Delta x_m} \leq 2 \end{cases} \tag{I-22}
$$

to insure that the local effective mesh Reynolds number is no greater than two. This result has been extended for generalized tensor equations and the appropriate dissipation terms for the continuity and momentum equations have been incorporated by Gibeling et al. (Ref. I-5) into the present version of the UTRC Navier-Stokes computer code.

A second type of artificial damping which is a fourth-order dissipation term has been suggested by Beam and Warming (Ref. I-9) to damp small wavelength disturbances. In the present formulation an explicit fourth-order damping term was added directly to the fundamental difference scheme, Eq. (I-16), as follows:

$$
(A + \Delta t \, \mathscr{L}) \, \psi^{n+1} = \Delta t \left[\mathscr{D}(\phi^n) + S^n \right] + \sum_{m=1}^{3} (\Delta y^m)^4 \, \frac{\omega_m}{8} \, \frac{\partial^4 \phi^n}{\partial (y^m)^4} \tag{I-23}
$$

This dissipation term is treated explicitly to retain the block tridiagonal matrix structure of the finite difference form of the governing equations.

NUMERICAL RESULTS FOR FLOW PAST A CIRCULAR CYLINDER

Under the present effort implicit time-marching Navier-Stokes solutions have been computed for symmetric, two-dimensional flows, at Reynolds numbers (based on diameter) of forty and eighty, past a circular cylinder (Fig. 1). In both cases the free stream Mach number was set equal to 0.2. The circular cylinder case is a convenient example because it represents a relatively simple geometry and both experimental data and other numerical solutions are available for comparison (cf. Ref. I-10). In particular, Gibeling, Shamroth, and Eiseman (Ref. I-5) have computed the flow past a circular cylinder at a Reynolds number of forty using the present numerical method. These authors considered the density and contravariant velocity components as dependent variables and did not use artificial fourth-order dissipation (cf. Eq. (I-23)) in their calculations. However, they later modified the Navier-Stokes computer code to consider density and the physical velocity components as dependent variables and introduced fourth order dissipation into the calculation procedure in order to compute flows past a symmetric Joukowski airfoil (Ref. I-5). Circular cylinder calculations are repeated here both to test the current version of the Navier-Stokes computer code, and so that the present investigators could gain experience in working with the code by applying it to a simple external flow configuration.

Due to symmetry results are computed for only the upper half-plane of the flow field using a 35 x 35 mesh embedded in a polar coordinate system. The outer boundary of the computational region was taken to be fifteen diameters from the cylinder center. A nonuniform grid spacing in physical space is applied with points along radial lines concentrated near the cylinder boundary and points on the circumferential lines concentrated near the front and rear stagnation points. Mesh points are distributed according to the relations

$$\Theta(i\Delta\theta) = \pi/2 - \pi/2 \, \tanh\left\{ D_\theta \left[1 - 2(i-1)\Delta\theta/\pi \right] \right\} / \tanh D_\theta, \quad i = 1,\ldots,I \quad \text{(I-24a)}$$

$$R(j\Delta r) = 30 - 29 \, \tanh\left\{ D_r \left[1 - (j-1)\Delta r \right] \right\} / \tanh D_r, \quad j = 1,\ldots,J \quad \text{(I-24b)}$$

where $\Delta\theta = \pi/(I-1)$, $\Delta r = 1/(J-1)$, $D_\theta = 0.75$, and $D_r = 2.7$ are damping constants for the Θ and R directions, respectively, and $I = J = 35$. The coordinate distributions, Eqs. (I-24), are special cases of the Roberts boundary layer transformation (Ref. I-11) and are shown plotted in Fig. 2.

The potential flow past a circular cylinder with a compressibility correction on density is specified as the initial flow field for the present viscous time marching solutions with the exception that the initial velocity on the surface of the cylinder is set equal to zero. Thus, the initial conditions are as follows:

$$\rho\big|_{t=0} = \left[1 + M_r^2 (1 - \gamma M_r^2 / 4)/2\right] / \left[1 + (M_r v)^2 (1 - \gamma (M_r v)^2 / 4)/2\right] \quad \text{(I-25a)}$$

$$v(1)\big|_{t=0} = -(1 + R^{-2}) \sin\Theta, \qquad R \neq 1 \quad \text{(I-25b)}$$

$$= 0, \qquad R = 1$$

$$v(2)\big|_{t=0} = (1 - R^{-2}) \cos\Theta \quad \text{(I-25c)}$$

where $v(1)$ and $v(2)$ are the physical velocity components in the R and Θ - directions, respectively and v is the magnitude of the velocity. The implicit time marching solutions are constrained to satisfy the following steady boundary conditions. Symmetry conditions are applied on the stagnation streamlines; i.e.,

$$\partial\rho / \partial\Theta = v(1) = \partial v(2) / \partial\Theta = 0, \qquad \text{on } \Theta = 0, \pi \quad \text{(I-26)}$$

thus permitting calculations to be restricted to the upper half-plane of the flow. The velocity and normal pressure gradient, $\partial p/\partial n$, is set equal to zero at the cylinder surface. This condition is required to determine a value of density at the surface and in the present case of constant total temperature, this condition is equivalent to $\partial\rho/\partial n = 0$. Therefore

$$\partial\rho / \partial R = v(1) = v(2) = 0, \text{ on } R = 1 \quad \text{(I-27)}$$

Finally, velocity and density are set to their inviscid values over the upstream three quarters of the outer boundary while first derivatives of the physical velocity components are set to zero and the pressure is set to its inviscid value over the remainder of the far-field boundary; i.e.,

$$\rho = \rho\big|_{t=0}, v(1) = v(1)\big|_{t=0}, v(2) = v(2)\big|_{t=0}, \quad \text{(I-28)}$$

$$\text{on } R = 30, \pi/4 < \Theta < \pi$$

and

$$\partial v(1)/\partial R = \partial v(2)/\partial R = 0,$$

(I-29)

$$\rho = p\Big|_{t=0} \Big/ \Big\{ A + B\Big[v^2(1) + v^2(2) \Big] \Big\}, \qquad \text{on } R = 30, \ 0 \le \theta \le \pi/4$$

The last condition follows from Eqs. (I-3) and (I-8) with $g_{12} = 0$ due to orthogonality.

At this point it is convenient to review the solution procedure using the circular cylinder problem as a vehicle to illustrate the method of incorporating the boundary conditions into the finite difference approximation. The foregoing steady state boundary conditions on the lines $\theta = 0$ and π and $R = 1$ and 30 can each be expressed in the form

$$\mathcal{D}_{BC}\psi^{n+1} = -\mathcal{D}_{BC}\phi^n + S^n$$

(I-30)

where $\mathcal{D}_{BC}$ is a matrix operator containing derivatives in the coordinate directions and S^n is a column vector function of ϕ^n. Hence the intermediate solution, ψ^*, after the nth time step of the alternating direction implicit procedure, is calculated on the circumferential lines, $R\,(j\Delta r) = \text{constant}$, $j = 2, \ldots, J-1$, as a solution of the equation set

$$\mathcal{D}_{BC}\Big|_{1,j}\,\psi^*_{1,j} = -\mathcal{D}_{BC}\Big|_{1,j}\,\phi^n + S^n_{1,j}$$

(I-31a)

$$(A + \Delta t\,\mathcal{L}_1)_{i,j}\,\psi^*_{i,j} = \Delta t\Big[\mathcal{D}_1{}^n + \mathcal{D}_2{}^n + S^n\Big]_{i,j}, \quad i = 2, \ldots, I-1$$

(I-31b)

$$\mathcal{D}_{BC}\Big|_{I,j}\,\psi^*_{I,j} = \mathcal{D}_{BC}\Big|_{I,j}\,\phi^n$$

(I-31c)

After approximating derivatives at boundaries by three point finite difference expressions, a block tridiagonal system of linear equations of the form (cf. Eq. (I-21))

22

$$b_{1,j}^n \, \psi_{1,j}^* + c_{1,j}^n \, \psi_{2,j}^* + a_{1,j}^n \, \psi_{3,j}^* = d_{1,j}^n \tag{I-32a}$$

$$a_{i,j}^n \, \psi_{i-1,j}^* + b_{i,j}^n \, \psi_{i,j}^* + c_{i,j}^n \, \psi_{i+1,j}^* = d_{i,j}^n \quad , i = 2, \ldots, I-1 \tag{I-32b}$$

$$c_{I,j}^n \, \psi_{I-2,j}^* + a_{I,j}^n \, \psi_{I-1,j}^* + b_{I,j}^n \, \psi_{I,j}^* = d_{I,j}^n \tag{I-32c}$$

results. Values of $\psi*$ are determined by using Gaussian elimination methods to solve this system of equations. Similarly, the viscous flow field at the $(n + 1)$th time level, ψ^{n+1}, is obtained as a solution of the equations

$$\mathcal{B}_{BC}\Big|_{i,1} \, \psi_{i,1}^{n+1} = -\mathcal{B}_{BC}\Big|_{i,1} \, \phi_{i,1}^n + S_{i,1}^n \tag{I-33a}$$

$$(A + \Delta t \, \mathcal{L}_2)_{i,j} \, \psi_{i,j}^{n+1} = A_{i,j} \, \psi_{i,j}^* \quad , j = 2, \ldots, J-1 \tag{I-33b}$$

$$\mathcal{B}_{BC}\Big|_{i,J} \, \psi_{i,J}^{n+1} = \mathcal{B}_{BC}\Big|_{i,J} \, \phi_{i,J}^n \tag{I-33c}$$

on the radial lines, $\Theta(i\Delta\theta) = $ constant, $i = 2, \ldots I-1$, after spatial difference approximations are introduced to express the foregoing equations in block tridiagonal form. The viscous solution evolves from the inviscid flow field, ψ^0, until the difference between the flows at two successive time steps, N and $N + 1$, satisfies an imposed convergence criterion. Specifically, the maximum value over the entire field of the absolute difference between the dependent variables at successive time steps must be less than some small number, ϵ; i.e.,

$$\| \phi^{N+1} - \phi^N \| = \max_{\begin{pmatrix} i=1,\ldots,I \\ j=1,\ldots,J \\ k=1,\ldots,3 \end{pmatrix}} \left| \phi_k^{N+1} - \phi_k^N \right| \le \epsilon \, , \tag{I-34}$$

Here the subscript k refers to the kth component of the column vector ϕ. In the solution procedure the magnitude of the time step at the nth time level, $n = 1, \ldots, N$, is a variable parameter which depends on the value of $\| \phi^n - \phi^{n-1} \|$.

In the present study implicit time-marching Navier-Stokes solutions were advanced through 160 and 200 time steps for circular cylinder flows at Reynolds numbers of 40 and 80, respectively. The dimensionless time step used in these calculations varied between 0.15 and 0.5. Artificial fourth order dissipation was at first applied for the circular cylinder calculations, but was found to lead to diverging solutions and spurious results in the far field. Hence, the only artificial viscosity term used below was that based on the mesh Reynolds number criterion, Eq. (I-22). The computations were carried out on the UTRC Univac 1110 computer system and the computing time for the nonorthogonal form of the governing equations used for the circular cylinder flows is approximately 0.95 CPU minutes per time step or 7.8×10^{-4} CPU minutes per grid point per time step. Selected results from the present calculations for flow past a circular cylinder are described below.

The variation of the minimum pressure and the separation angle, Θ_s, with time is depicted in Fig. 3 for the Re = 40 case and in Fig. 4 for the Re = 80 case. After 160 time steps the separation angle reaches a value of 51.4^o for Re = 40. This is to be compared with values of 50.0^o, 52.5^o, 53.7^o, and 53.9^o obtained by Kawaguti (Ref. I-12), Apelt (Ref. I-13), Kawaguti and Jain (Ref. I-14) and Son and Hanratty (Ref. I-15). The development of the pressure distribution around the surface of the cylinder with time is shown in Fig. 5 for Re = 40 and in Fig. 6 for Re = 80. The time history plots, Figs. 3 through 6 reveal that although the implicit time-marching results appear to be converging, steady state solutions have not been achieved even after a considerable number of iterations or time steps. The maximum difference between dependent variables at successive time steps (cf. Eq. (34)) is of the order of 2×10^{-3} after 160 (Re = 40) and 200 (Re = 80) time steps. In addition, as will be seen below, the results after 160 time steps for the Reynolds number of forty case are not in good agreement with previous calculations or experimental measurement.

The present prediction of surface pressure distribution for Re = 40 after 160 time steps is compared with the predictions of Son and Hanratty (Ref. I-15), Kawaguti (Ref. I-12) and Gibeling, Shamroth, and Eiseman (Ref. I-5) in Fig. 7. Note that the angular coordinate, Θ, is equal to 180° at the front stagnation point. The Kawaguti pressure coefficient prediction was given relative to the rear stagnation point pressure and in Fig. 7 the Kawaguti rear stagnation point pressure was arbitrarily set at the Son and Hanratty value. The predictions of Refs. (I-15) and (I-12) were both obtained from solutions of the incompressible Navier-Stokes equations while the solution of Ref. I-5 and the present solution were obtained from the compressible equations with Mach number equal to 0.2. As is clear from Fig. 7, the agreement between the present predictions and those of Refs. I-5, I-12, and I-15 is rather poor with the present analysis over predicting the pressure over most of cylinder surface. In addition, the time history plots, Figs. 3 and

5, indicate that with continued iteration the pressure prediction based on the present procedure would deviate still further from previous results. Indeed, the results achieved with the present method after 80 time steps are in better agreement with the previous predictions than those achieved after 160 time steps. Wake centerline velocity distributions for Reynolds numbers of 40 and 80, based on the present analysis, along with the predictions of Kawaguti (Ref. I-12) and Gibeling et al (Ref. I-5), and the experimental measurements of Coutanceau and Bouard (Ref. I-10) for a Reynolds number of 40 are depicted in Fig. 8. Again the agreement between the data and the present results for Re = 40 is not good. As a final illustration of the results of the present calculations, the velocity profiles for Re = 40 and Re = 80 at several azimuthal locations are shown in Fig. 9 along with the predictions of Gibeling, Shamroth, and Eiseman (Ref. I-5) for Re = 40. Substantial differences can be observed between the results of these two analyses.

Based on the present study the performance of the implicit time-marching Navier-Stokes computer code has not been satisfactory. Converged solutions could not be obtained for simple low Reynolds number flows and the results after a considerable number of time steps are not in good agreement with those of previous analyses or experimental data. In contrast, Gibeling, Shamroth and Eiseman (Ref. I-5) used essentially the same version of the Navier-Stokes computer code and reported a converged solution for the flow past a circular cylinder at Re = 40 after only 80 time steps, and their results are in very good agreement with the previous incompressible analyses of Refs. I-12 and I-15 and the experimental data of Ref. I-10. The major difference between the present analysis and that of Ref. I-5 is that physical velocity components are treated as the dependent variables here, while contravariant velocity components were assumed as dependent variables in the former analysis. The modifications to the Navier-Stokes computer code to accomplish this change of dependent variables were made by Gibeling et al in order to decrease numerical truncation errors. At this time the reason for the discrepancies between the present results and those of the Ref. I-5 study are not apparent, but further studies to clarify this situation seem warranted. In this regard information concerning the time step distribution and convergence criterion used in the previous analysis (Ref. I-5) as well as intermediate results for pressure and velocity would be most useful.

TWO-DIMENSIONAL CASCADE FLOWS

A major objective of the present study has been to further develop the implicit time-marching Navier-Stokes computer code so that this code could be applied to the calculation of viscous flow through cascades. In particular, a solution scheme for cascade flow fields has been formulated and the relevant subroutines of the Navier-Stokes computer code have been modified to accommodate this scheme. The solution formulation is based on the use of the two-dimensional, curvilinear cascade coordinate system developed by Eiseman (Ref. I-16). This system consists of coordinate loops surrounding each blade and radial coordinate lines normal to the blade surface. The outermost loop is constructed so that cascade periodicity conditions can be applied without interpolation between grid points. The coordinates are orthogonal on the airfoil surface, but gradually become nonorthogonal away from the airfoil. Mesh points can be packed in regions of large solution gradients and little restriction is placed on airfoil camber and spacing. At present, Eiseman's coordinate generator can accurately produce systems for inviscid studies; however, further refinements are required to produce the higher order smoothness necessary for viscous cascade analyses. An example of an Eiseman cascade coordinate system is depicted in Fig. 10.

Consider two dimensional flow past an isolated airfoil or a blade in cascade and a coordinate system consisting of coordinate loops surrounding the airfoil (or blade) and radial coordinate lines emanating from the airfoil (or blade) surface and terminating on an outermost coordinate loop. The sketch in Fig. 11 will be used to illustrate the computational procedure for both the flow past an isolated airfoil and a blade in cascade. In the former case the reader should envision the outermost coordinate loop ABCDEFGH in Fig. 11 as lying in the far field while in latter, he should envision the outermost loop as consisting of cascade periodic boundaries, CD and GH, and front, HC, and rear, DG, endcaps which lie in the far field. In both cases the innermost coordinate loop coincides with the airfoil (or blade surface).

For the isolated airfoil an intermediate solution, ψ^*, of the ADI form of the Navier-Stokes equations, between the n and n + 1 time levels is obtained by solving the direction - 1 equation, i.e., Eq. (I-18a) with $\mathcal{D}_3 = 0$ or Eq. (I-31), along the coordinate loops with the exception of the loop which coincides with the airfoil surface and the outermost or far-field loop. The starting radial line for the direction - 1 calculation can be chosen arbitrarily. The solution at the n + 1 time level, ψ^{n+1}, is then obtained by solving the direction - 2 equation; i.e., Eq. (I-18b) with $\psi^{**} = \psi^{n+1}$ or Eq. (I-33b), of the ADI representation on each radial line subject to the appropriate boundary conditions at the airfoil surface and

at the far-field boundary; e.g., the conditions at $R = 1$ (Eqs. (I-27)) and $R = 30$ (Eqs. (I-28 and I-29)) for the circular cylinder problem. Blade passage flows can be calculated in a similar manner, but conditions must be imposed at the periodic boundaries (CD and GH in Fig. 11) in lieu of far-field conditions. These conditions are that the density and velocity must be equal at periodic points (e.g., C and H, and D and G in Fig. 11) and values of these flow variables on the periodic boundaries must be solutions of the Navier-Stokes equations. The blade-to-blade periodicity requirement indicates that solutions of the direction - 2 equations for ψ^{n+1} should proceed simultaneously along radial lines which terminate at two periodic points on the outermost coordinate loop.

If $\vec{e}_{(i)}$, $i = 1, 2$, denotes the natural basis of tangent vectors to the loopwise and radial coordinate curves, then

$$\vec{e}_{(i)}^{\,j} = \delta_i^{\,j} \tag{I-35a}$$

$$\vec{e}_{(i)} \cdot \vec{e}_{(j)} = g_{ij} \tag{I-35b}$$

where the superscript in Eq. (I-35a) refers to the contravariant component of the base vector $\vec{e}_{(i)}$. The components of the unit outward normal vector to the loopwise-coordinate lines are obtained by solving the equations

$$\vec{n} \cdot \vec{e}_{(1)} = g_{11} \, n^1 + g_{12} \, n^2 = 0 \tag{I-36a}$$

and

$$\| \vec{n} \| = g_{ij} \, n^i \, n^j = 1 \tag{I-36b}$$

It follows that

$$n^1 = -g_{12} / (J \sqrt{g_{11}}) \tag{I-37a}$$

$$n^2 = \sqrt{g_{11}} / J \tag{I-37b}$$

Then since the velocity must be equal at upper and lower periodic points

27

$$\left(\vec{v}\cdot\vec{e}_{(1)}\right)^{U} = \left(v^{1}g_{11} + v^{2}g_{21}\right)^{U} = -\left(v^{1}g_{11} + v^{2}g_{21}\right)^{L} = -\left(\vec{v}\cdot\vec{e}_{(1)}\right)^{L} \quad \text{(I-38a)}$$

$$\left(\vec{v}\cdot\vec{n}\right)^{U} = \left(J\,v^{2}/\sqrt{g_{11}}\right)^{U} = -\left(J\,v^{2}/\sqrt{g_{11}}\right)^{L} = -\left(\vec{v}\cdot\vec{n}\right)^{L} \quad \text{(I-38b)}$$

The blade-to-blade periodicity conditions on density and the physical velocity components then have the form (cf. Eq. (I-8)):

$$\rho^{U} = \rho^{L} \quad \text{(I-39a)}$$

$$\left[\sqrt{g_{11}}\,v(1) + g_{12}\,v(2)/\sqrt{g_{22}}\right]^{U} = -\left[\sqrt{g_{11}}\,v(1) + g_{12}\,v(2)/\sqrt{g_{22}}\right]^{L} \quad \text{(I-39b)}$$

$$\left[J\,v(2)/\sqrt{g_{11}\,g_{22}}\right]^{U} = -\left[J\,v(2)/\sqrt{g_{11}\,g_{22}}\right]^{L} \quad \text{(I-39c)}$$

It is possible to construct an implicit solution scheme for the *Navier-Stokes equations at a cascade periodic boundary;* however, such a scheme would entail rather complicated changes to the Navier-Stokes computer code. Hence, in the present effort an explicit scheme has been adopted. Thus the form of the governing equations applied at a periodic boundary follows from Eq. (I-16) with $\beta = 0$; i.e.,

$$A\psi^{n+1} = \Delta t\left[\mathbf{g}^{n} + S^{n}\right] \quad \text{(I-40)}$$

In addition, since the radial coordinate lines of the cascade coordinate system do not possess continuous derivatives at periodic boundaries (see Figs. 10 and 11) the use of one sided difference approximations for derivatives in the radial coordinate direction is indicated. If necessary, an implicit solution scheme using central differences could be adopted in future studies. Construction of an implicit scheme would involve straightforward, albeit very tedious, coding changes. The introduction of central difference approximations in the radial direction is contingent on future refinements in the cascade coordinate system described in Ref. (I-16).

With the foregoing ideas in mind the Navier-Stokes computer code has been modified to encompass the following solution scheme for the blade passage problem. Intermediate solutions, ψ^{*}, of the direction - 1 equations are obtained in the counterclockwise direction along the coordinate loops

with the exception of the blade surface and outermost loops. These solutions start from the first radial coordinate line which terminates on the front end cap (i.e., at point A in Fig. 11) and proceed around the blade to the radial coordinate line which terminates at the end of the upper periodic boundary (i.e., point H in Fig. 11). Solutions at the n + 1 time level, ψ^{n+1}, are then obtained by solving the direction - 2 equations along the radial coordinate lines subject to solid surface boundary conditions at the blade, upstream and downstream far-field conditions on the front, AB in Fig. 11, and rear, EF, endcaps, respectively, of the outer coordinate loop ABCDEFGH (Fig. 11), explicit Navier-Stokes solutions on the lower periodic boundary, CD, and blade-to-blade periodicity conditions on the upper periodic boundary GH. Solutions along radial lines which terminate at periodic points on the outer boundary proceed simultaneously. Although this is not strictly required in the present formulation, which uses explicit Navier-Stokes solutions at the lower periodic boundary, it has been incorporated so that possible future improvements, i.e., implicit procedures at the lower boundary can be readily incorporated.

As part of the current effort, the modifications to the matrix inversion, boundary condition, general coefficient, and spatial differentiation sub-routines of the implicit time-marching Navier-Stokes computer code, to incorporate the foregoing formulation have been completed. The changes to the existing code have been accomplished in a concise manner involving the addition of only one new subroutine and only a limited number of additional input parameters. The code modifications have been checked out by calculating the symmetric flow past an isolated circular cylinder using symmetry conditions, which are similar in form to cascade periodicity conditions (i.e., symmetry involves only a change of sign in Eq. (I-39c)) at the endpoints of radial lines extending above and below the cylinder. Computed results for this case after five time steps are virtually identical to those obtained using the usual isolated body, far-field boundary conditions for the circular cylinder calculations. Such agreement indicates that the modifications to the Navier-Stokes code required to treat cascade periodicity conditions have been successfully completed and that this code is ready to accept the cascade geometry module developed by Eiseman (Ref. I-16). However, before the geometry module is incorporated into the Navier-Stokes code the coordinate generator must be further developed to provide the higher order smoothness required for viscous flow studies.

REFERENCES - PART I

I-1.   Briley, W. R. and H. McDonald: An Implicit Numerical Method for The
        Multidimensional Compressible Navier-Stokes Equations. United
        Aircraft Research Laboratories Report M911363-6, November 1973.

I-2.   Douglas, J. and J. E. Gunn: A General Formulation of Alternating
        Direction Methods. Numerische Math., Vol. 6, pp. 428-453, 1964.

I-3.   Briley, W. R., H. McDonald, and H. J. Gibeling: Solution of the
        Multidimensional Navier-Stokes Equations by a Generalized Implicit
        Method. United Technologies Research Center Report R75-911363-17,
        January 1976.

I-4.   Richtmeyer, R. D. and K. W. Morton: Difference Methods for Initial
        Value Problems. John Wiley & Sons, 1967.

I-5.   Gibeling, H. J., S. J. Shamroth and P. R. Eiseman: Analysis of
        Strong-Interaction Dynamic Stall for Laminar Flow on Airfoils.
        United Technologies Research Center Report R77-912030-17, July 1977.

I-6.   Aris, R.: Vectors, Tensors, and the Basic Equations of Fluid
        Mechanics. Prentice-Hall, Inc., 1962.

I-7.   Isaacson, E., and H. B. Keller: Analysis of Numerical Methods.
        John Wiley and Sons, Inc., New York, 1966.

I-8.   Roache, P. J.: Computational Fluid Dynamics. Hermosa Publisher,
        Albuquerque, New Mexico, 1972.

I-9.   Beam, R., and R. F. Warming: An Implicit Finite Difference
        Algorithm for Hyperbolic Systems in Conservation-Law-Form. Journal
        of Computational Physics, Vol. 22, pp. 87-110, September 1976.

I-10.   Coutanceau, M., and R. Bouard: Experimental Determination of the
        Main Features of the Viscous Flow in the Wake of a Circular
        Cylinder in Uniform Translation. Part 1. Steady Flow. Journal of
        Fluid Mechanics, Vol. 79, pp. 231-256, 1977.

I-11.   Roberts, G. O.: Computational Meshes for Boundary Layer Problems.
        Proceedings of the Second International Conference on Numerical
        Methods in Fluid Dynamics, Springer Verlag, New York, p. 171, 1971.

I-12.   Kawaguti, M.: Numerical Solution of the Navier-Stokes Equations for
        the Flow Around a Circular Cylinder at Reynolds Number 40. Journal
        of the Physical Society of Japan, Vol. 8, pp. 747-757, 1953.

REFERENCES - PART I (Cont'd)

I-13.   Apelt, C. J.: The Steady Flow of a Viscous Fluid Past a Circular
        Cylinder at Reynolds Numbers 40 and 44. Aeronautical Research
        Council R. & M. No. 3175, 1958.

I-14.   Kawaguti, M., and P. C. Jain: Numerical Study of a Viscous Fluid
        Flow Past a Circular Cylinder. Journal of the Physical Society
        of Japan, Vol. 21, p. 2055.

I-15.   Son, J. S. and T. J. Hanratty: Numerical Solution for the Flow
        Around a Cylinder at Reynolds numbers of 40, 200 and 500. Journal
        of Fluid Mechanics, Vol. 35, pp. 369-386, 1969.

I-16.   Eiseman, P. R.: A Coordinate System for a Viscous Transonic Cascade
        Analysis. United Technologies Research Center Report, February 1977.

PART II

A VISCID/INVISCID INTERACTION APPROACH

FOR HIGH REYNOLDS NUMBER TRAILING

EDGE FLOW

LIST OF SYMBOLS - PART II

a	reference length
C	Chapman-Rubesin viscosity constant
C_p	constant pressure specific heat
$\bar{e}$	unit vector
h	coordinate scale factor
H	total enthalpy
H_s	surface height in bottom deck variables
j	geometry index: $j = 0$ 2-D flow; $j = 1$ axisymmetric flow
$\bar{j}$	Cartesian coordinate unit vector
M	Mach number
n	transposed normal coordinate
N	transposed stretched normal coordinate
$\mathcal{O}$	asymptotic ordering symbol
p	static pressure
P	inner deck pressure
q	heat transfer
r, r_o	transverse coordinate and surface radii respectively
Re	Reynolds number
s	transposed longitudinal coordinate
t	position of coordinate system, inner variables
t_o	position of coordinate system

LIST OF SYMBOLS - PART II (Cont'd)

T	static temperature
u	longitudinal velocity
U	inner deck or inviscid longitudinal velocity
v	normal velocity, transposed coordinates
V	inner deck normal velocity
w	normal velocity
x	longitudinal coordinate
X	inner deck longitudinal coordinate
y	normal coordinate
Y	inner deck normal coordinate
α	inner region ramp angle parameter
γ	ratio of specific heats
δ	inner deck displacement thickness
ϵ	perturbation parameter
κ	longitudinal surface curvature
λ	Blasius constant
μ	viscosity coefficient
φ	inclination angle with horizontal axis
ρ	density
σ	Prandtl number
τ	shear stress
θ	trailing edge angle

34

LIST OF SYMBOLS - PART II (Cont'd)

Subscripts

e	inviscid edge values
F.P.	flat plate solution
m	matching region values
T.E.	trailing edge location
ν	viscous or main deck region
W	wall values
x, y, z	coordinate direction
∞	free stream value

35

GENERAL APPROACH

The problem of base flow separation off the trailing edge region of
airfoils (i.e., trailing edge stall) causes difficulty in analytically
predicting the losses and loading in turbomachinery applications. Upon close
inspection, it is obvious that this flow and its attendent difficulties are
very similar to those encountered in predicting surface separation bubbles,
the main difference here being that reattachment takes place on a slip line
instead of on a solid surface. While it has long been clear that classical
boundary layer theory is inadequate for predicting separated flows, recent
analytical developments indicate that a consistent and reliable analytical
model can be constructed using somewhat less than the full Navier-Stokes
equations. Additionally, careful analysis of experimental data suggests that
the effect of the stalled flow trailing edge separation bubble on the flow
field is confined to the immediate region in and about the trailing edge
region. This observation indicates that to capture the trailing edge flow
phenomenon it is only necessary to modify the classical approach (i.e.,
inviscid flow plus boundary layer theory) in the immediate vicinity of the
trailing edge. Thus, while methods based on the application of the full
Navier-Stokes equations to the entire flow field will surely be formally
applicable, alternate, simpler approaches are now available.

For separation bubble flows, all of the simpler analytical models to
date contain two common features: first, in the viscous region diffusion
effects normal to the streamlines dominate all others and; second the inviscid
flow field represents flow over a surface formed by thickening the original
shape with the local viscous region's displacement thickness. Variations on
this approach involve either a composite of these two layers (the thin layer
approximation, the parabolized approach, etc.) or a substructure delineation
(the triple deck, or the multi-deck approaches). In either case, successful
modeling of separation bubble flows has been achieved and it remains now to
apply and extend these concepts to stalled subsonic and transonic trailing
edge regions in turbomachinery applications. This is the overall goal of the
present study with specific interest in the formulation of the two layer,
interacting laminar boundary layer model of this flow field. A companion
study has also been conducted on the development and demonstration of numer-
ical techniques for solving such flows for the supersonic trailing edge
problem - the results of which will be summarized here.

The general approach to be employed here follows closely the work
of Melnik, Chow, and Mead (Ref. II-1) who developed an interacting boundary
layer model for high Reynolds number flow past isolated airfoils. As depic-
ted in Fig. 12, the overall flow field model is rather conventional except
that an interaction model is employed to bridge the trailing edge region

36

where the blade boundary layer transists to a wake flow. The major element
of this approach is that for high Reynolds number the laminar viscous flow is
assumed to influence the inviscid flow field principally through displacement
effects and is represented by the displacement thickness as added to the air-
foil surface and wake centerlines. Thus, the major elements of the flow are:
(1) an inviscid flow outside the thin viscous regions here taken to be gov-
erned by the potential flow equations as applied to cascades; (2) a weakly
interacting boundary layer region over the forward portion of the blade; (3)
a weakly interacting wake region aft of the trailing edge region; and (4) a
strongly interacting trailing edge region where the local pressure levels
must be established along with the viscous solution. Coupling of these four
flows produces a boundary value problem in the flow direction that Melnik
et al. (Ref. II-1) have shown can be solved with iterative techniques.
Attention here will be directed at the solution of the strongly interacting
trailing edge region where Melnik et al. used approximate techniques to
solve for attached flows only. The separated (or stalled) trailing edge
problem will be addressed here using recently developed interacting boundary
layer concepts (see Refs. II-2, 6). Attention will be focused on the laminar
flow past symmetric sharp trailing edges, as depicted in Fig. 13, with trail-
ing edge angles large enough to cause the boundary layer to separate off the
surface and reattach on a wake slip line.

THE TRAILING EDGE FLOW MODEL

The details of the flow field for the trailing edge region are given in Fig. 13. Here the basic inviscid flow is that of flow into and out of a concave corner. This strongly deaccelerating flow field forces the incoming boundary layer to grow, deflect the inviscid stream, and finally separate from the surface and reattach along the wake – producing a displacement surface that smooths the sharp corner's influence on the local inviscid flow field (see Fig. 14).

The analytical model for this flow field is taken directly from that already proved to be applicable for flow into a compression corner made up of two solid walls. Vatsa and Werle (Ref. II-4), Jenson, Burggraf, and Rizzetta (Ref. II-7) and Burggraf et al (Ref. II-11) have clearly shown that the interacting boundary layer concept provides a rational approximation for such flows and this concept will be carried over directly here. The principle governing equations for the viscous region are formally recovered from the Navier-Stokes equations using the formalism of higher order boundary layer theory (Ref. II-8) to identify the displacement thickness corrections to the flow equations.

The basic approach taken here is similar to that first set down by Van Dyke (Ref. II-9) except that here no attempt is made to filter out the higher-order effects into separate linear problems. Van Dyke has given a statement of the full Navier-Stokes equations for two-dimensional or axisymmetric flow in terms of the coordinates x and y with all distances referenced to a length, a, velocities to U_∞, pressure to $\rho_\infty U_\infty^2$, density to ρ_∞, temperature to U_∞^2/C_p, enthalpy to U_∞^2, and viscosities to the value of μ at $T = U_\infty^2/C_p$. With these definitions the characteristic Reynolds number becomes

$$Re = \rho_\infty U_\infty a/\mu (U_\infty^2/C_p) = 1/\epsilon^8 \qquad (II-1)$$

where ϵ becomes the principle perturbation parameter for an asymptotic analysis of the separated flow region using the concepts developed by Stewartson (Ref. II-10).

For present purposes we approach the full equations with the assumption that in a vanishingly small region near the surface, a region of order ϵ^4 thick, all flow properties except the normal velocity component v are of order one – v itself being of order ϵ^4.

Without loss of generality the coordinate system used here will be placed placed along a smooth surface always located near the line of zero longitudinal

38

velocity as shown in Fig. 15. It will be shown later that within the framework of an analytical model applicable for asymptotically large Reynolds number, this arbitrariness in the coordinate definition will be totally acceptable.

The governing equations are recovered by introducing a stretching of the viscous region normal coordinate, y_ν, to give a boundary layer coordinate y as

$$y = y_\nu / \epsilon \qquad (II-2a)$$

and retaining the longitudinal coordinate scale as

$$x = x_\nu \qquad (II-2b)$$

and using unsubscripted variables to designate the flow properties in the viscous region as follows:

longitudinal velocity:	$u_\nu(x_\nu, y_\nu; \epsilon) = u(x, y, \epsilon)$	$(II-3a)$
normal velocity:	$w_\nu(x_\nu, y_\nu; \epsilon) = \epsilon^4 w(x, y; \epsilon)$	$(II-3b)$
density:	$\rho_\nu(x_\nu, y_\nu; \epsilon) = \rho(x, y, \epsilon)$	$(II-3c)$
pressure:	$p_\nu(x_\nu, y_\nu; \epsilon) = p(x, y; \epsilon)$	$(II-3d)$
static enthalpy:	$T_\nu(x_\nu, y_\nu; \epsilon) = T(x, y, \epsilon)$	$(II-3e)$
total enthalpy:	$H_\nu(x_\nu, y_\nu; \epsilon) = H(x, y; \epsilon)$	$(II-3f)$

The coordinate scale factors are designated as

$$h_x = 1 + \epsilon^4 \kappa y \equiv h \qquad (II-4a)$$

$$h_y = 1 \qquad (II-4b)$$

$$h_z = (r_0 + \epsilon^4 y \cos\theta)^j \equiv r^j \qquad (II-4c)$$

Introducing these definitions into the full equations, keeping all terms up to second order, and invoking the asymptotic matching principle to determine the interaction with the inviscid flow field, gives the following for plane ($j = 0$) or axisymmetric flows ($j = 1$).

continuity:

$$\frac{\partial}{\partial x}\left(\rho r^{j}u\right) + \frac{\partial}{\partial N}\left(\rho h r^{j}w\right) = 0 \tag{II-5a}$$

longitudinal momentum:

$$\rho\left[u\,\frac{\partial u}{\partial x} + w\,\frac{\partial hu}{\partial y}\right] - \rho_m\left(U_e/h\right)\frac{\partial}{\partial x}\left(U_e/h\right) +$$

$$\frac{\partial}{\partial x}\left[\int_y^\infty \frac{h_y}{h^3}\left(\rho_m U_e^2 - \rho h^2 u^2\right)dy\right] = \frac{1}{hr^j}\,\frac{\partial}{\partial y}\left(r^j h^2 \tau\right) \tag{II-5b}$$

where

$$\tau \equiv \mu\left(\frac{\partial u}{\partial y} - u h_y/h\right) \tag{II-5c}$$

total enthalpy:

$$\rho\left[u\,\frac{\partial H}{\partial x} + hw\,\frac{\partial H}{\partial y}\right] = \frac{1}{r^j}\,\frac{\partial}{\partial y}\left[hr^j(q + u\tau)\right] \tag{II-5d}$$

40

where

$$q \equiv \mu/\sigma \, \frac{\partial T}{\partial y} = \mu/\sigma \left[\frac{\partial H}{\partial y} - u \, \frac{\partial u}{\partial y} \right] \qquad (II\text{-}5e)$$

Also the viscosity law is given as:

$$\mu = f(T)$$

where $f(T)$ represents any appropriate temperature viscosity law with

$$T = H - u^2/2 \qquad (II\text{-}6)$$

The final two relations needed are derived from the matching conditions as

$$P_m + \int_y^\infty \frac{h_y}{h^3} \left[\rho_m U_e^2 - \rho h^2 u^2 \right] dy = \frac{\gamma-1}{\gamma} \, \rho \left(H - \frac{u^2}{2} \right) \qquad (II\text{-}7a)$$

and

$$p_m/p_e = (\rho_m/\rho_e)^\gamma = \left[1 + (U_e^2/2)(H_e - U_e^2/2)(1 - 1/h^2) \right]^{\frac{\gamma}{\gamma-1}} \qquad (II\text{-}7b)$$

The edge conditions, U_e and H_e identified above, are to be obtained
from the inviscid flow field corrected for displacement thickness effects.
This issue will be addressed later in this section with attention here
directed toward application of the above general equations to the trailing
edge problem and identification of appropriate boundary conditions.

41

The first simplification invoked here for the trailing edge problem involves restriction to the two dimensional case, i.e., taking $j = 0$ in the above equations. The second simplification comes about through elimination of the curvature induced effects identified through the scale factor h. This is accomplished on two bases. First, in regions of weak interaction, such as far ahead and aft of the trailing edge, the geometry of the coordinate line is flat and thus its curvature is zero. Second, in regions of strong interactions as occur near the trailing edge point, the formal ordering analysis for asymptotically large Reynolds number indicates that these terms will be of secondary importance. To demonstrate this point it is first necessary to show that the strong interaction equations derived from the asymptotic triple deck approach are subsets of the interacting boundary layer equations presented above. Burggraf, Rizzeta, Werle and Vatsa (Ref. II-11) have proven this point numerically, while Vatsa (Ref. II-12) and Vatsa and Werle (Ref. II-4) have shown that the introduction of the triple deck scaling laws into the interacting boundary layer equations leads directly to the correct subscale equations for strong interaction regions.

Thus, for example, for trailing edge angles $\alpha = \mathcal{O}(\epsilon^2)$ it is found that within a region $x - x_{TE} = \mathcal{O}(\epsilon^3)$, $y = \mathcal{O}(\epsilon)$; i.e., the bottom deck region within which the separation bubble is contained, the dependent variables scale as[*]

$$u = \mathcal{O}(\epsilon) \qquad (II-8a)$$
$$w = \mathcal{O}(1/\epsilon) \qquad (II-8b)$$
$$\Delta p = \mathcal{O}(\epsilon^2) \qquad (II-8c)$$
$$\rho = \mathcal{O}(1) \qquad (II-8d)$$
$$H = \mathcal{O}(1) \qquad (II-8e)$$
$$\mu = \mathcal{O}(1) \qquad (II-8f)$$

In addition, since in the present approach the coordinate axis is placed on a surface necessarily contained within this region, it follows that, the coordinate location, $t_o(x) = \mathcal{O}(\epsilon^5)$ and its curvature $\kappa = \mathcal{O}(1/\epsilon)$. With these scalings, the dominate terms of the governing equations for the bottom deck can be identified for the continuity equations as

continuity: $\qquad\qquad\qquad\qquad\qquad\qquad\qquad\qquad$ (II-9a)
$$\frac{\partial u}{\partial x} + \frac{\partial w}{\partial y} = 0$$

---

[*] See the following section of this report for a detail description of the scaling laws discussed here.

energy:
$$u \frac{\partial H}{\partial x} + w \frac{\partial H}{\partial y} = \frac{\mu}{\sigma} \frac{\partial^2 H}{\partial y^2} \tag{II-9b}$$

The limit form of the longitudinal momentum equation is dependent on the scaling law for the edge velocity U_e, which is established in the outer most portion of the strong interaction region ($y = \mathcal{O}(\epsilon^3)$). In this region, one finds that the viscous perturbation to $U_e^2 = \mathcal{O}(\epsilon^2)$. With this the longitudinal momentum Eq. II-5b reduces to

$$u \frac{\partial u}{\partial x} + w \frac{\partial u}{\partial y} - U_e \frac{dU_e}{dx} = \frac{\partial^2 u}{\partial y^2} \tag{II-9c}$$

A similar study of the appropriate scalings in the middle deck region of the strong interaction process would again reveal that the curvature terms were of secondary importance, but that here density and temperature variations were of lead order. Thus a composite set of equations can be established for the two regions as

$$\frac{\partial \rho u}{\partial x} + \frac{\partial \rho w}{\partial y} = 0 \tag{II-10a}$$

$$\rho \left[u \frac{\partial u}{\partial x} + w \frac{\partial u}{\partial y} \right] - \rho_e U_e \frac{dU_e}{dx} = \frac{\partial}{\partial y} \left(\mu \frac{\partial u}{\partial y} \right) \tag{II-10b}$$

$$\rho \left[u \frac{\partial H}{\partial x} + w \frac{\partial H}{\partial y} \right] = \frac{\partial}{\partial y} \left[\frac{\mu}{\sigma} \frac{\partial T}{\partial y} + u \mu \frac{\partial u}{\partial y} \right] \tag{II-10c}$$

which are merely the classical boundary layer equations with edge properties adjusted for interaction effects.

The boundary conditions for the present equations can be set down directly as

$$y \rightarrow \infty \; ; \; u \rightarrow U_e \; \text{and} \; H \rightarrow H_e \qquad \text{(II-11)}$$

$$y = -t_o(x)/\epsilon^4 \equiv -t(x) \qquad \text{(II-12a)}$$

On the blade surface: $x \leq x_{T.E.}$; $u = w = 0$, $H = H_w$ $\qquad$ (II-12b)

On the wake centerline: $x > x_{T.E.}$;

$$\overline{j} \cdot \overline{V} = 0 \qquad \text{(II-12c)}$$
$$\overline{j} \cdot \nabla H = 0 \qquad \text{(II-12d)}$$
$$\overline{j} \cdot \nabla (\overline{i} \cdot \overline{V}) = 0 \qquad \text{(II-12e)}$$

where $\overline{j}$ is the vertical unit vector.

Following Jenson et al (Ref. II-7) these latter conditions can be considerably simplified through use of Prandtl's Transposition Theorem. Thus define

$$N = y + t(x) = n/\epsilon^4 \qquad \text{(II-13a)}$$

so that the innermost boundary conditions are placed at $N = 0 = n$.

In addition define

$$s = x \qquad \text{(II-13b)}$$

and

$$v = w + u\frac{dt}{dx} = w + ut' \qquad \text{(II-13c)}$$

so that

$$\frac{\partial}{\partial x} = \frac{\partial}{\partial s} + t'\frac{\partial}{\partial N} \qquad \text{(II-14a)}$$

and

$$\frac{\partial}{\partial y} = \frac{\partial}{\partial N} \qquad \text{(II-14b)}$$

With these definitions the governing equations remain unchanged in form and thus become

$$\frac{\partial \rho u}{\partial s} + \frac{\partial \rho v}{\partial N} = 0 \qquad\qquad (II-15a)$$

$$\rho \left[u \frac{\partial u}{\partial s} + v \frac{\partial u}{\partial N} \right] - \rho_e U_e \frac{dU_e}{ds} = \frac{\partial}{\partial N} \left(\mu \frac{\partial u}{\partial N} \right) \qquad\qquad (II-15b)$$

and

$$\rho \left[u \frac{\partial H}{\partial s} + v \frac{\partial H}{\partial N} \right] = \frac{\partial}{\partial N} \left[\frac{\mu}{\sigma} \frac{\partial T}{\partial N} - \mu u \frac{\partial u}{\partial N} \right] \qquad\qquad (II-15c)$$

The boundary conditions for these equations are straightforward on the surface, but can be considerably simplified over those given in Eqs. (II-12b) through (II-12d) for the wake centerline.

Referring to Fig. 15, consider the condition that

$$\overline{j} \cdot \overline{V} = 0 \qquad\qquad (II-16a)$$

or

$$w_\nu \sin \phi - u_\nu \cos \phi = 0 \qquad\qquad (II-16b)$$

Thus

$$w_\nu = \epsilon^4 w = u_\nu \tan \phi = -\frac{dt_o}{ds} u_\nu = -\epsilon^4 t' u \qquad\qquad (II-16c)$$

which from Eq. (II-13c) give that along the slip line,

$$n = 0 \qquad\qquad v = 0 \qquad\qquad (II-16d)$$

45

Evaluation of the normal derivative conditions is somewhat more tedious. The gradient operator is given as

$$\nabla = \frac{\overline{e}_x}{h} \frac{\partial}{\partial x} + \overline{e}_y \frac{\partial}{\partial y} \qquad \text{(II-17a)}$$

so that

$$\overline{j} \cdot \nabla = \frac{-\sin\theta}{h} \left[\frac{\partial}{\partial y} - \tan\theta \frac{\partial}{\partial n} \right] + \cos\theta \frac{\partial}{\partial n} \qquad \text{(II-17b)}$$

Thus the wake centerline condition on total enthalpy becomes

$$\frac{\partial H}{\partial n} = - \frac{t_o'}{h + t_o'^2} \frac{\partial H}{\partial s} \qquad \text{(II-18a)}$$

and since

$$\overline{i} \cdot \overline{V} = u / \cos\theta \qquad \text{(II-18b)}$$

then

$$\frac{\partial u}{\partial n} = - \frac{t_o'}{h + t_o'^2} \left[\frac{\partial u}{\partial s} - \kappa t_o' u \right] \qquad \text{(II-18c)}$$

These relations can be simplified by noting that in the weak interaction region $t_o \rightarrow 0$ whereas in the strong interaction region, the bottom deck scaling laws apply. Applying Eqs. (II-8a) through (II-8f) to Eqs. (II-17a) and (II-17b) leads to the result that for $n = 0$, $s > s_{T.E.}$ the appropriate boundary conditions are given as

46

$$\frac{\partial H}{\partial n} = 0 \qquad \qquad \text{(II-19)}$$

$$\frac{\partial u}{\partial n} = 0 \qquad \qquad \text{(II-20)}$$

It remains now only to establish the analytical basis for establishing the edge properties, U_e, p_e, etc. Both the weak and strong interaction theories indicate that this can be accomplished employing the effective displacement surface (see Refs. II-4, 12, 13, and 15 for example) obtained by the simple addition of the boundary layer and/or wake displacement thickness to the original inviscid flow shape. This is the approach that will be employed here.

THE HIGH REYNOLDS NUMBER PROBLEM - THE TRIPLE DECK EQUATIONS*

While the interacting boundary layer problem formulated above is expected to have application over a very wide range of Reynolds numbers, it has been shown by Vatsa and Werle** (Ref. II-4) that these equations reduce to a relatively simple and instructive form as the Reynolds number increases. In particular, Vatsa and Werle were able to show that the interacting boundary layer equations contain the subscale structure (the triple deck structure) identified by Stewartson (Ref. II-10), and Jenson, Burggraf and Rizzeta (Ref. II-7) for interacting flows. Of particular interest here is the application of this concept to the supersonic compression corner problem as depicted in Fig. 16. Through identification of the subscalings shown near the hinge line and of the ramp angle, a distinguished limit solution to the Navier-Stokes equations for Re $\gg$ 1 was identified that captured the interaction and separation phenomena. As such the solutions are as fundamentally important to the field of separation flow theory as the Blasius solution is to attached flow theory. An additional benefit of this approach is that it is found to reduce the parametric dependence of the problem from four (M_∞, Re_∞, T_w/T_∞, θ) to one, α, where

$$\alpha \equiv \lambda^{-1/2} \left[\frac{Re_\infty}{C(M_\infty{}^2 - 1)} \right]^{1/4} \tag{II-21}$$

Thus these equations provide a convenient and useful test vehicle for developing solution methods and demonstrating concepts while providing meaningful quantitative separated or stalled flow solutions.

The approach used by Vatsa and Werle (Ref. II-4) follows directly from that of Jenson et al (Ref. II-7) in that the scaling laws identified for strong interactions by Stewartson (Ref. II-10) are applied in the near region of a geometric obstruction - in this case, a compression corner. The principle region of interest here is the bottom deck of Fig. 16, which can be identified in terms of scaled dependent variables, X and Y, given as:

$$x - x_{T.E} = s - s_{T.E} \equiv \lambda^{-5/4} \left[\frac{\epsilon C^{1/8}}{(M_\infty{}^2 - 1)^{1/8}} \right]^3 (T_w/T_\infty)^{3/2} X \tag{II-22a}$$

---

*   The work presented here and in the following two sections concerning the asymptotic Triple Deck equations, their numerical solution algorithm, and the demonstration of results were performed under a United Technologies sponsored project outside the scope of the contract requirements. They are included here to demonstrate the utility of this approach.

** These results have also been discussed by Burggraf (Ref. II-6) and will be appearing shortly in Ref. II-11.

$$n = y_\nu + t_0 = \epsilon^4 N \equiv \lambda^{-3/4} \; \frac{\left[\epsilon C^{1/8}\right]^5}{(M_\infty^2 - 1)^{1/8}} \; (T_w/T_\infty)^{3/2} \; Y \qquad (II\text{-}22b)$$

The dependent variable scalings for this region have been discussed briefly in an earlier section of this report and are given here in detail as:

longitudinal velocity:

$$u_\nu = u \equiv \lambda^{1/4} \; \frac{\epsilon C^{1/8}}{(M_\infty^2 - 1)^{1/8}} \; (T_w/T_\infty)^{1/2} \; U \qquad (II\text{-}23a)$$

normal velocity:

$$W_\nu + u_\nu t_0' = \epsilon^4 v \equiv \lambda^{3/4} \; \frac{\left[\epsilon C^{1/8}\right]}{(M_\infty^2 - 1)^{1/8}} \; (T_w/T_\infty)^{1/2} \; V \qquad (II\text{-}23b)$$

static pressure:

$$p - p_\infty \equiv \lambda^{1/2} \left[\frac{\epsilon C^{1/8}}{(M_\infty^2 - 1)^{1/8}} \right]^2 \; P \qquad (II\text{-}23c)$$

With the introduction of these asymptotic scale laws and those for the local inviscid flow into the interacting boundary layer equations given by Eqs. (II-15a) through (II-15c) above, Vatsa and Werle (Ref. II-4) were able to identify the dominant terms of the interacting boundary layer equations for high Reynolds number strong interactions as

continuity:

$$\frac{\partial U}{\partial x} + \frac{\partial V}{\partial Y} = 0 \qquad (II\text{-}24a)$$

49

longitudinal momentum:

$$U \frac{\partial U}{\partial x} + V \frac{\partial U}{\partial x} + \frac{dP}{dy} = \frac{\partial^2 U}{\partial Y^2} \tag{II-24b}$$

and the energy equation is found to be uncoupled from these fundamental equations. These equations are identical to those derived from the Navier-Stokes equations by Jenson et al (Ref. II-7). The viscous/inviscid interaction law for the asymptotic problem is a simplified version of that for the interacting boundary layer problem and is given as

$$P = \frac{d}{dx}(\delta + H_s) \tag{II-25a}$$

where H_s is the surface height given here for the ramp in inner deck variables as

$$H_s = 0 \quad \text{for } X \leq 0 \tag{II-25b}$$

$$H = \alpha X \quad \text{for } X > 0 \tag{II-25c}$$

and s is a displacement thickness like function given as

$$\delta = \lim_{Y \to \infty} (Y - U) \tag{II-25d}$$

It has been demonstrated that these equations provide the same solution at high Reynolds number as that of the interacting boundary layer equations by Burggraf, Rizzeta, Werle and Vatsa (Ref. II-11)[*] with the significant results repeated here for completeness. For a fixed value of $\alpha = 2.5$, Figs. 17 and 18 compare separated flow solutions of the interacting boundary layer equations with solutions of the fundamental equations given above.

---

[*] Also see Refs. II-4, 6, and 11 for further discussion of this point.

50

It is clearly seen that both the surface pressure and skin friction distributions obtained from the interacting boundary layer approach systematically approach the triple deck solutions as the Reynolds number increases - thus verifying the utility of the fundamental triple deck version of the governing equations for study of the interacting boundary layer model of the trailing edge stall problem. For this case the boundary condition aft of the trailing edge is obtained by applying the scaling laws above to Eqs. (II-16d) and (II-18d) to obtain:

$$X > 0, \ Y = 0$$

$$V = 0 \qquad\qquad\qquad\qquad\qquad \text{(II-26a)}$$

$$\frac{\partial U}{\partial Y} = 0 \qquad\qquad\qquad\qquad\qquad \text{(II-26b)}$$

To provide insight into the nature of the trailing edge flow field, solutions of Eqs. (II-24) through (II-26) have been obtained using numerical techniques outlined in the following section with a discussion of the results presented in the subsequent section.

NUMERICAL METHOD - THE TRIPLE DECK EQUATIONS

The numerical method applied to solve the trailing edge problem described above will be outlined briefly below. The approach represents an extension of the concept originally developed by Werle and Vatsa (Ref. II-3) for the full interacting boundary layer equations. The method used here directly follows the application and generalization of this technique to the triple deck equations by Napolitano, Werle, and Davis (Ref. II-2) for subsonic and supersonic separated flow past protuberances and compression corners. The basic approach uses a marching type implicit finite difference scheme to solve the continuity and momentum Eqs. (II-4a) and (II-4b) with nonlinearities approximated using previous station data. The pressure interaction effect enters through the pressure gradient term of Eq. (II-4b) and is coupled to the local velocity through Eqs. (II-5a) through (II-5b). This effect is accommodated through introduction of a time-like relaxation scheme wherein dP/dX of Eq. (II-4b) is replaced with the term $dP/dX - d\delta/dt$ and the solution marched in time to achieve $d\delta/dt = 0$. A simple superposition technique is employed to determine the simultaneous solution of the conservation and interaction equations at a given station so that computational efficiency is maintained.

For completeness two versions of the numerical algorithm were employed here. The first of these was a slight modification of the numerical algorithm presented in Ref. II-2 and as such was first order accurate in the longitudinal direction, ΔX. A second order accurate version of the numerical method was also available and has been applied here. A brief outline of the principle features of each algorithm is given below.

The First Order Method

The algorithm employed here is virtually identical to that developed by Napolitano, Werle, and Davis (Refs. II-2 and II-15) for subsonic and supersonic flows with several changes as required to accommodate the details of the flow structure in the trailing edge region. These changes for the present supersonic case represent generalizations of those concepts employed by Napolitano et al, (Refs. II-2 and II-15) to accommodate sharp corner effects in subsonic flows. The changes are identified below with reference to the appropriate sections and equations of Reference II-15.

(i)   the continuity equation (II-24a) solution technique was modified one station aft of the trailing edge in accordance with Section IV-2 and Eq. (4.13) of Ref. II-15.

52

(ii)   the numerical representation of the normal convection term of Eq. (II-24b) was modified according to Section IV-2 and Eq. (4.14) of Ref. II-15.

(iii)   at a given time level, the pressure gradient term dP/dx appearing in Eq. (II-24b) above was obtained from previous time level solutions using Eq. (4.1) of Ref. II-15.

(iv)   the numerical approach employed in Section IV-4 of Ref. II-15 to solve the interaction law and thus update the pressure gradient estimate was employed here. However, the Cauchy integral terms for subsonic flow were replaced by the appropriate algebraic relation for supersonic flows.

A final modification was made to provide more accurate representation of the local pressure levels after the solutions were completed. This was found necessary principally for the flat plate trailing edge problem where singular gradients and thus large truncation errors were encountered. Thus, the pressure at a typical point, point 2, was given in terms of previous station values, point 1, from Eq. (II-25a) as

$$P_2 = \frac{(\delta_2 + H_{s_2}) - (\delta_1 - H_{s_1})}{\Delta x} + \frac{\Delta x}{2}\left(\frac{dP}{dx}\right)_2 \qquad (II-27)$$

The Second Order Method

In an effort to provide very accurate numerical baseline solutions so that a valid independent assessment of the analytical model could be achieved untainted by numerical complications, an available second order accurate (in ΔX) numerical algorithm was also applied to the present problem. The algorithm employs an approach very similar to that presented in Ref. II-15 except that here the first order accurate implicit windward differencing used in the longitudinal direction for the momentum equation was replaced by a second order accurate Crank-Nicolson scheme. Similarly the accuracy of the continuity equation solution was upgraded to second order in ΔX by centering the difference equation between two longitudinal stations. To avoid large numerical errors due to anticipated jump discontinuities in the flow variables several of the formally second order accurate central difference approximations were relieved to a first order level at a single station immediately aft of the trailing edge.

RESULTS AND DISCUSSION - THE TRIPLE DECK PROBLEM

Solution to the high Reynolds number form of the interacting boundary
layer equations (the triple deck equations) were first obtained for super-
sonic flow into a compression corner as depicted in Fig. 19. As such, this
geometry only differs from that of the trailing edge in that the center line
symmetry condition is replaced by a zero slip condition aft of the corner
point. An essentially exact solution is available for this problem from the
work of Rizzetta (Ref. II-13)*, thus allowing a basis for assessing the cur-
rent algorithms. Figure 20 gives a comparison of the normalized wall shear
stress and surface pressures for a reduced ramp angle of $\alpha = 2.5$ — a case
for which separation and flow recirculation was encountered. As shown in the
figure both of the present algorithms provide reasonable approximations to the
exact results showing a pressure rise ahead of the corner up to a "plateau"
level as the flow separates over the corner followed by a second pressure rise
to the ramp pressure level during flow reattachment. Quite naturally it is
found that the second order accurate (in ΔX) algorithm is more accurate than
its first order accurate counterpart. These solutions were obtained on a
UNIVAC 1110 computer in approximately 30 seconds of CPU time for grid sizes of
70 (in X) by 26 (in Y) and a convergence criterion that the average variation
per iteration be less than 10^{-4}. As shown in the figure the accuracy was
found to be somewhat insensitive to the normal grid size (ΔY) apparently due
to the second order level of the algorithm for the normal direction. In order
to verify the utility of the present algorithms, solutions were also obtained
across the full range of α with the resulting surface pressure and shear dis-
tributions given in Figs. 21 and 22 respectively. These results clearly
show the significant and systematic growth of the interaction region ahead of
the corner as the ramp angle is increased.

The algorithm as employed to perform the ramp calculations above, was
modified for the trailing edge problem through a single adjustment aft of
the corner point to replace the no surface slip condition with the wake center-
line symmetry condition of Eqs. (II-26). Solutions were then obtained for
a range of α up to and including the stall (separation) condition. Comparison-
sons are first given here for the flat plate ($\alpha = 0$) case since Daniels (Ref.
II-14) has already provided very accurate solutions for this case which can
be used to assess the accuracy of the present algorithms. Figure 23 gives
a detailed assessment of the present results obtained from both the first and
second order (in ΔX) algorithms. Here the pressure distribution on the plate
surface up to the trailing edge is given along with the wake centerline pres-
sure distribution. For this geometry, interaction effects cause the pressure

---

* See also Refs. II-4, 6 and 11

54

to begin to drop far ahead of the trailing edge as it anticipates the abrupt boundary layer thinning aft of the trailing edge when the retarding influence of the surface no slip condition is relieved. Both the first and second order results essentially reproduce Daniels (Ref. II-14) results with the only significant difference occurring in the immediate vicinity of the trailing edge itself. The small oscillations observed in the centerline pressures for the second order algorithm and "kink" observed for the first order algorithm are caused by the extremely high acceleration of the flow immediately aft of the trailing edges. As shown in Fig. 24 these minor difficulties are eliminated as the grid spacing is refined with the resulting 1st order solution providing a "smoothed" version of the second order results near the trailing edge.

Solutions for the general trailing edge problem were then generated using both of the present algorithms. Figures 25 through 27 give the second order algorithm results for α up to 2.5 where stall took place. The pressure distributions over the airfoils and wake centerlines in the trailing edge regions are shown in Fig. 25. As the trailing edge angle, α increases, the wake effect is anticipated further forward on the airfoil surface in much the same manner as in the compression corner case. A detailed comparison of Figs. 22 and 25 indicates that the interaction effect is slightly less severe for the trailing edge problem then it is for the compression corner. The airfoil surface shear distributions for the region ahead of the trailing edge are given in Fig. 26 for the full range of α studied here. Comparison with Daniels (Ref. II-14) flat plate results are seen to be very good even in the immediate trailing edge region where the rapid acceleration in the wake region has caused a thinning of the viscous layer and subsequent increased shear. As the trailing edge angle was increased, the initial acceleration effect of the wake region (producing increased surface shear) changed to a deacceleration effect (producing decreased surface shear). The appearance of negative shear for $\alpha = 2.5$ signals the occurrence of reverse flow (i.e., a stalled trailing edge). The accompanying wake centerline velocity distributions for the same range of α are given in Fig. 27. Here comparison with Daniels (Ref.II-14) flat plate results show a slight loss in accuracy apparently due to the extremely rapid flow accelerations experienced at the trailing edge (Daniels shows that $\frac{\partial U}{\partial X} \to \infty$ as $X \to 0^+$). Fortunately, as the trailing edge angle was increased, this acceleration decreased until it finally reversed, indicating that a recirculating stalled-flow bubble was formed for $\alpha = 2.5$.

It was found that the computing time required for the second order algorithm to achieve a converged solution increased as the trailing edge angle increased. Whereas the solutions for $\alpha = 0$ were achieved in 1.5 minutes of CPU time, approximately 9 minutes were required for the $\alpha = 2.5$ case. Since the first order algorithm was observed to achieve convergence significantly faster than its second order counterpart, solutions were also obtained here

over a wide range of trailing edge angle using this algorithm. The resulting pressure distributions are shown in Fig. 28 for α up to 3. These results are essentially the same up to $\alpha = 2$ as those given in Fig. 25 for the second order algorithm but were obtained here in approximately one third of the computing time. For $\alpha = 2$, the difference in the results was found to be small and to diminish as the step size was reduced in the first order algorithm. Thus this algorithm provides a reliable and reasonably efficient method for solving stalled trailing edge flows and should be useful in the extension of the present approach to other flow regimes (i.e., subsonic flows, loaded airfoils, turbulent flows).

REFERENCES - PART II

II-1.   Melnik, R. E., R. Chow, and H. R. Mead: Theory of Viscous Transonic
        Flow Over Airfoils at High Reynolds Number. AIAA Paper No. 77-680,
        presented at the Tenth Fluid and Plasma Dynamics Conference, 1977.

II-2.   Napolitano, M., M. J. Werle, and R. T. Davis: A Numerical Technique
        for the Triple-Deck Problem. AIAA Paper 78-1133, presented at the
        11th AIAA Fluid and Plasma Dynamics Conference, June 1978.

II-3.   Werle, M. J., and V. N. Vatsa: A New Method for Supersonic Boundary
        Layer Separation. AIAA Journal, pp. 1491-1497, November 1974.

II-4.   Vatsa, V. N. and M. J. Werle: Quasi-Three-Dimensional Laminar
        Boundary Layer Separations in Supersonic Flows. ASME Journal of
        Fluids Engineering, December 1977, also see Quasi-Three-Dimensional
        Supersonic Viscid/Inviscid Interactions Including Separation Effects.
        Air Force Flight Dynamics Laboratory Report, AFF DL-TR-75-138,
        Wright Patterson AFB Ohio, November 1975.

II-5.   Carter, James E.: A New Boundary-Layer Interaction Technique for
        Separated Flows. NASA Tech Memo, 78690, June 1978.

II-6.   Burggraf, O.: Three Dimensional Viscous Interactions. Paper
        presented at the International Workshop on Viscous Interaction and
        Boundary Layer Separation, Ohio State University, Columbus, Ohio,
        August 16, 1976.

II-7.   Jenson, R., O. R. Burggraf, and D. Rizzetta: Asymptotic Solution
        for Supersonic Viscous Flow Past a Compression Corner. Proceedings
        4th International Conference on Numerical Methods in Fluid Mechanics,
        Lecture Notes in Physics, Vol. 35, Springer Verlag, 1975.

II-8.   Davis, R. T., M. J. Werle, and S. F. Wornom: A Consistent Formula-
        tion of Compressible Boundary-Layer Theory with Second-Order Curvature
        and Displacement Effects. AIAA Journal, Vol. 8, pp. 1701-1703,
        September 1970.

II-9.   Van Dyke, M.: Higher-Order Boundary Layer Theory. Annual Review of
        Fluid Mechanics, Vol. 1, pp. 265-292, 1969.

II-10. Stewartson, K.: Multistructured Boundary Layers on Flat Plates and
        Related Bodies. Advances in Applied Mechanics, Academic Press Inc.,
        Vol. 14, pp. 145-239, 1974.

REFERENCES - PART II (Cont'd)

II-11. Burggraf, O. R., D. Rizzetta, M. J. Werle, and V. N. Vatsa: Effects
        of Reynolds Number on Laminar Separation of a Supersonic Stream.
        Submitted to AIAA Journal for publication, 1977.

II-12. Vatsa, V. N.: Quasi-Three-Dimensional Viscid/Inviscid Interactions
        Including Separation Effects. PhD Dissertation, University of
        Cincinnati, Cincinnati, Ohio, 1975.

II-13. Rizzetta, D. P.: Asymptotic Solution for Two Dimensional Viscous
        Supersonic and Hypersonic Flows Past Compression and Expansion
        Corners. PhD Dissertation, Ohio State University, 1976.

II-14. Daniels, P. G.: Numerical and Asymptotic Solutions for the
        Supersonic Flow Near the Trailing Edge of a Flat Plate. Quarterly
        Journal of Mechanics and Applied Mathematics, Vol. XXVII, Part 2,
        pp. 175-191, 1974.

II-15. Napolitano, M., M. J. Werle, and R. T. Davis: Numerical Solutions
        of the Triple-Deck Equations for Supersonic and Subsonic Flow Past a
        Hump. University of Cincinnati Aerospace Engineering Department,
        Report No. AFL 78-6-42, June 1978.

CONCLUDING REMARKS

Two major areas have been investigated under the present effort. The first concerns the application of a numerical procedure for solving the compressible Navier-Stokes equations to cascade blade passage flows, and the second deals with the construction and numerical solution of an interacting boundary layer model for airfoil trailing edge flows.

Under the first part of the present effort an existing computer code, based on an alternating direction, implicit time marching solution of the general coordinate representation of the Navier-Stokes equations, has been modified to be applicable to the blade passage problem. In particular, the general coefficient, matrix inversion, boundary condition, and spatial differentiation subroutines of the existing code were modified to incorporate cascade blade-to-blade periodicity conditions. The latter consist of obtaining an explicit solution of the governing equations at one periodic boundary and specifying periodicity of density and velocity at the other periodic boundary.

Implicit time-marching Navier-Stokes solutions have been computed for flows past a circular cylinder at Reynolds numbers of forty and eighty. The convergence rate for this code was found to be slow. In particular, 160 time steps for the Re = 40 case and 200 time steps for Re = 80, with Δt varying between 0.15 and 0.5, were required to achieve a convergence level of 2×10^{-3} (c.f. Eq. (I-34). In addition, for the Re = 40 case pressure and velocity distributions after 160 time steps are not in good agreement with previous calculations or experimental data. Time history plots of the current calculations indicate that continued iteration would not improve the result comparisons. At present the reasons for the lack of agreement between present and previous calculations are not apparent, and further work (e.g., step size studies to interrogate truncation errors, investigation of different coordinate distributions, etc.) seems warranted to resolve this issue.

Under the second part of the present effort an interacting boundary layer model, incorporating the asymptotic triple deck concept, has been formulated for airfoil trailing edge flows. Attention is focused on the flow past symmetric, wedge-shaped trailing edges, with trailing edge angles large enough to cause flow separation from the airfoil surface and re-attachment on the wake slip line. The analytical model is taken directly from that already proved to be applicable for flow into a compression corner.

Numerical solutions to the triple deck version of this model have been obtained for the laminar supersonic case. Results determined for a 0° trailing edge angle (flat plate) were found to be in good agreement with those

obtained earlier by P. G. Daniels. Present calculations have been extended
over a range of trailing edge angles until a separated flow solution
("stalled" trailing edge) was achieved. Solutions have been obtained with
two different finite difference formulations. One is essentially second
order accurate while the other is first order accurate but provides faster
solutions. Accuracy studies indicate that the two formulations are producing
consistent results for the stalled trailing edge case. Although both attached
and separated supersonic trailing edge flows have been sucessfully calculated,
there are areas for possible improvements in the present numerical algorithms,
in particular, in treating flow discontinuities at the trailing edge, if
experimental comparisons indicate that such improvements are warranted.
Future work should also be directed at the extension of the current approach
to turbulent flows, lifting configurations and full cascade flow fields.
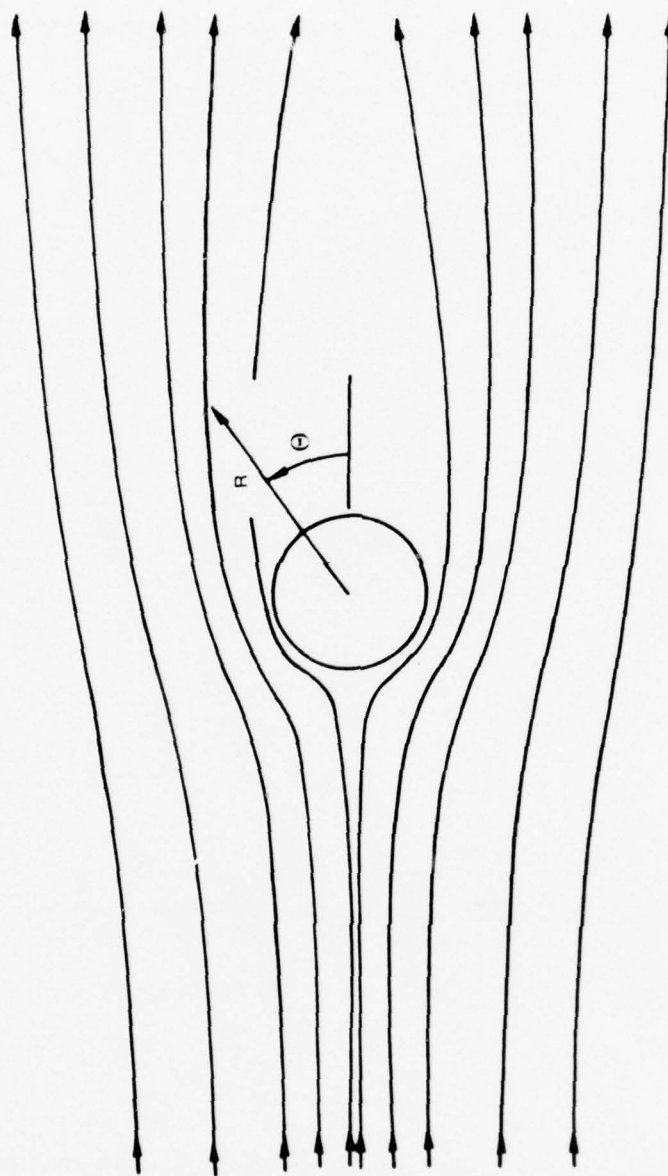
Figure 1—Flow Past a Circular Cylinder
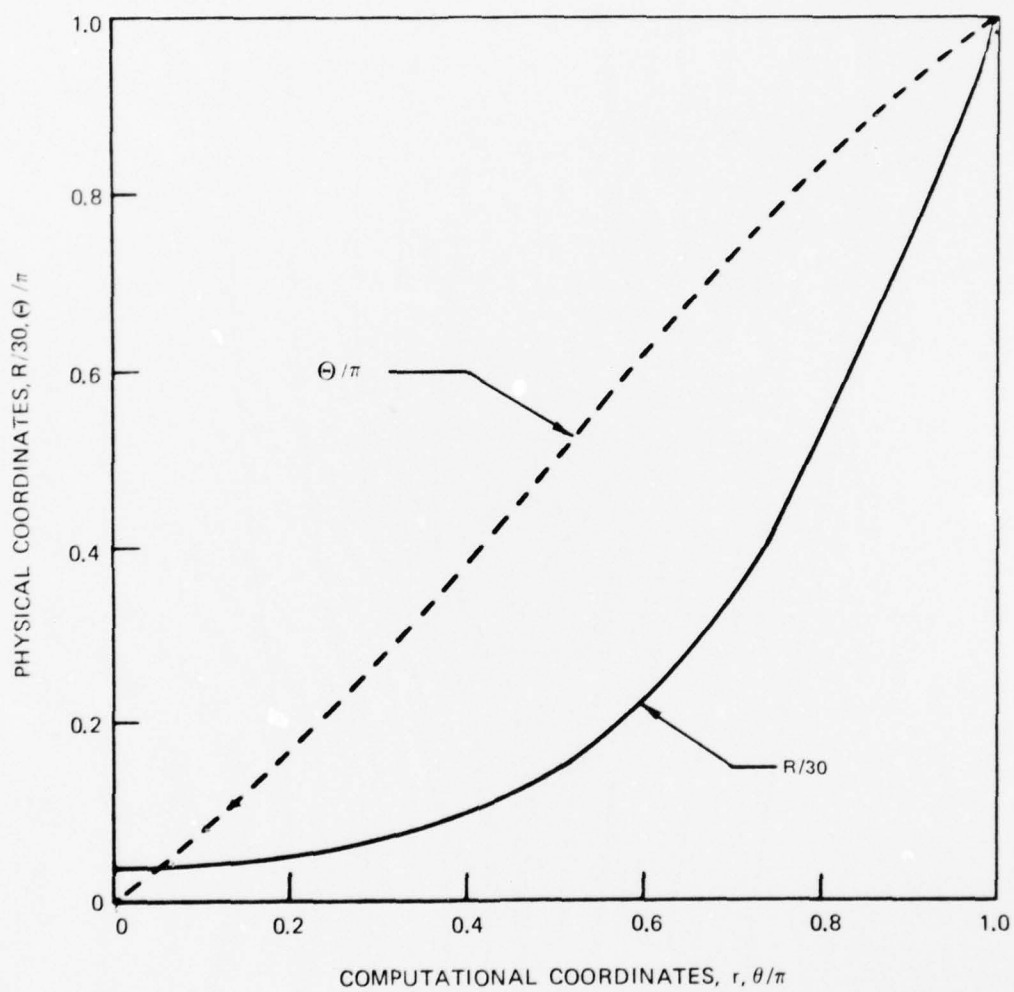
Figure 2—Coordinate Distributions for Circular Cylinder Flow Field Calculations
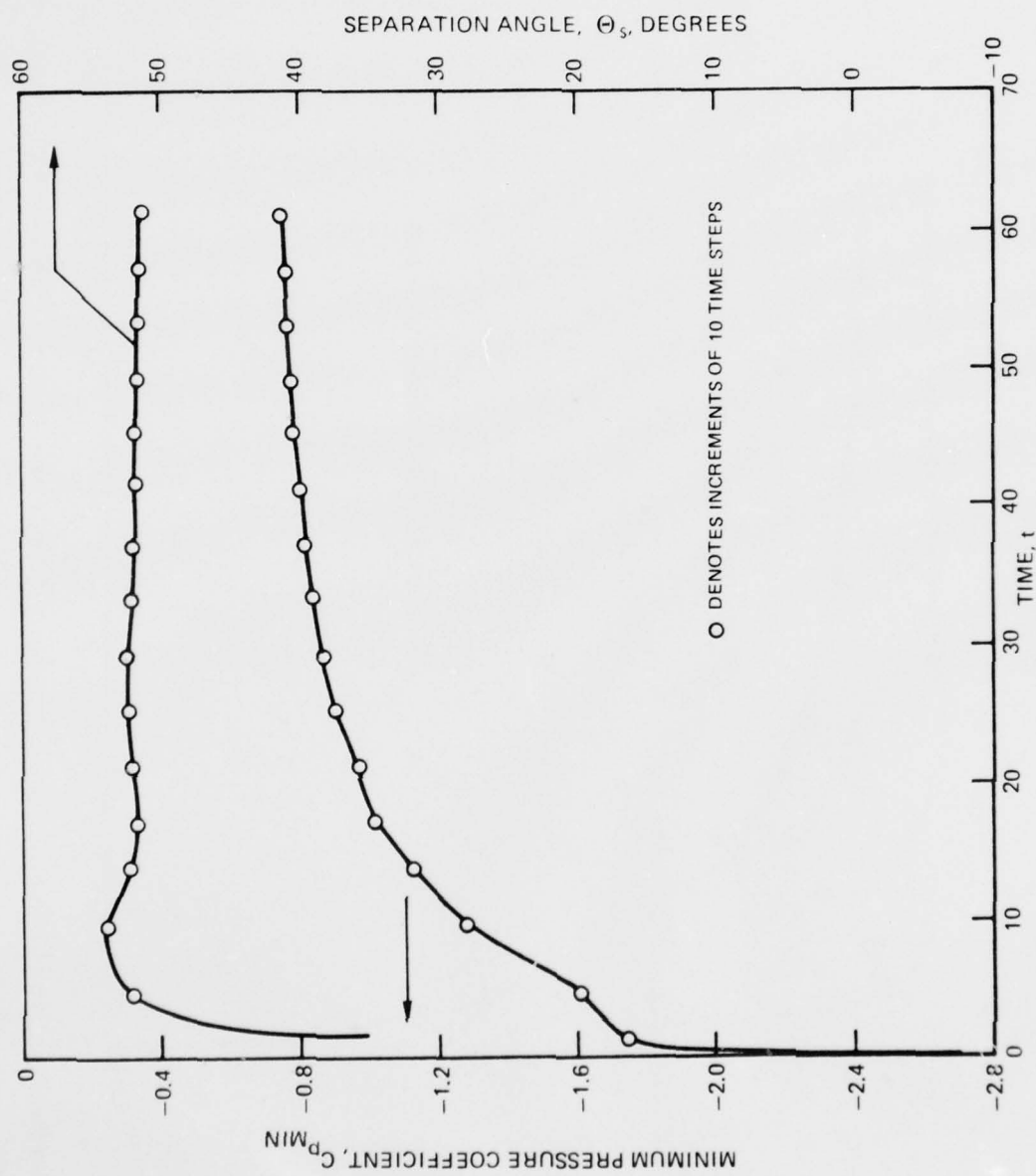
Figure 3—The Development of Minimum Surface Pressure and Separation Angle for Flow Past a Circular Cylinder at Re = 40

SEPARATION ANGLE, Θ_s, DEGREES

O DENOTES INCREMENTS OF 10 TIME STEPS

TIME, t

MINIMUM PRESSURE COEFFICIENT, $C_{p_{MIN}}$
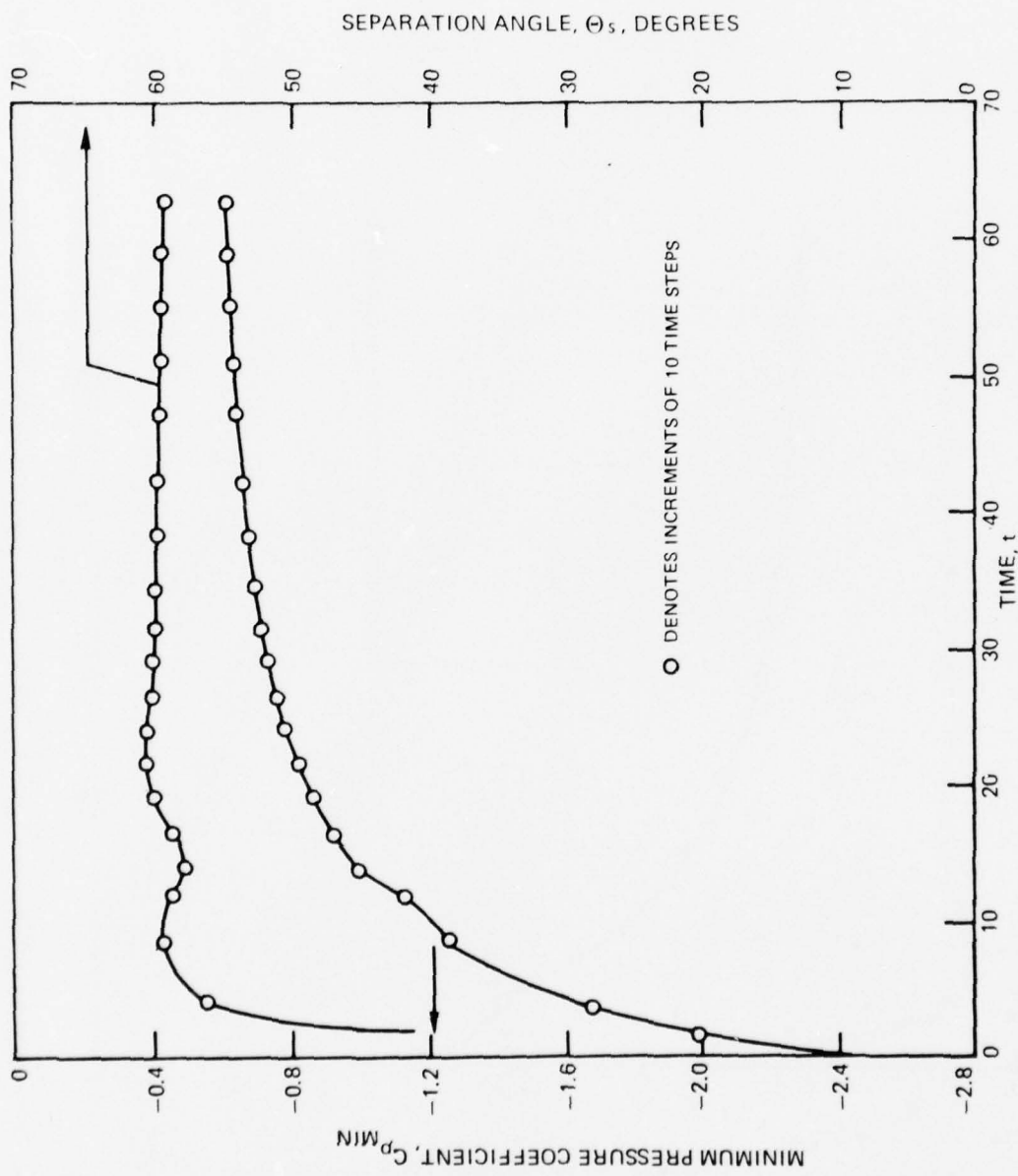
Figure 4—The Development of Minimum Surface Pressure and Separation Angle for Flow Past a Circular Cylinder at Re = 80

78-08-173-4

TIME, t	NUMBER OF TIME STEPS
13.8	40
29.3	80
45.3	120
61.3	160
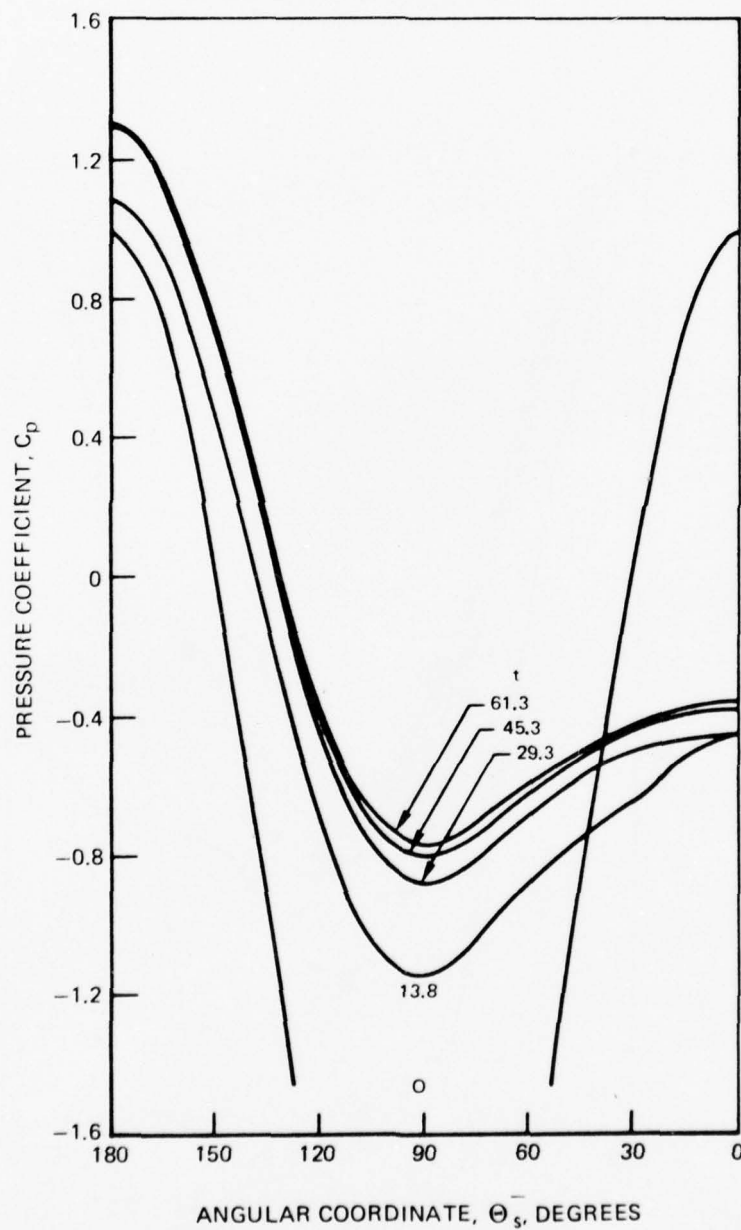
Figure 5—The Development of Surface Pressure with Time for Flow Past a Circular Cylinder at Re = 40

TIME, t	NUMBER OF TIME STEPS
11.9	40
21.5	80
31.5	120
47.0	160
62.6	200
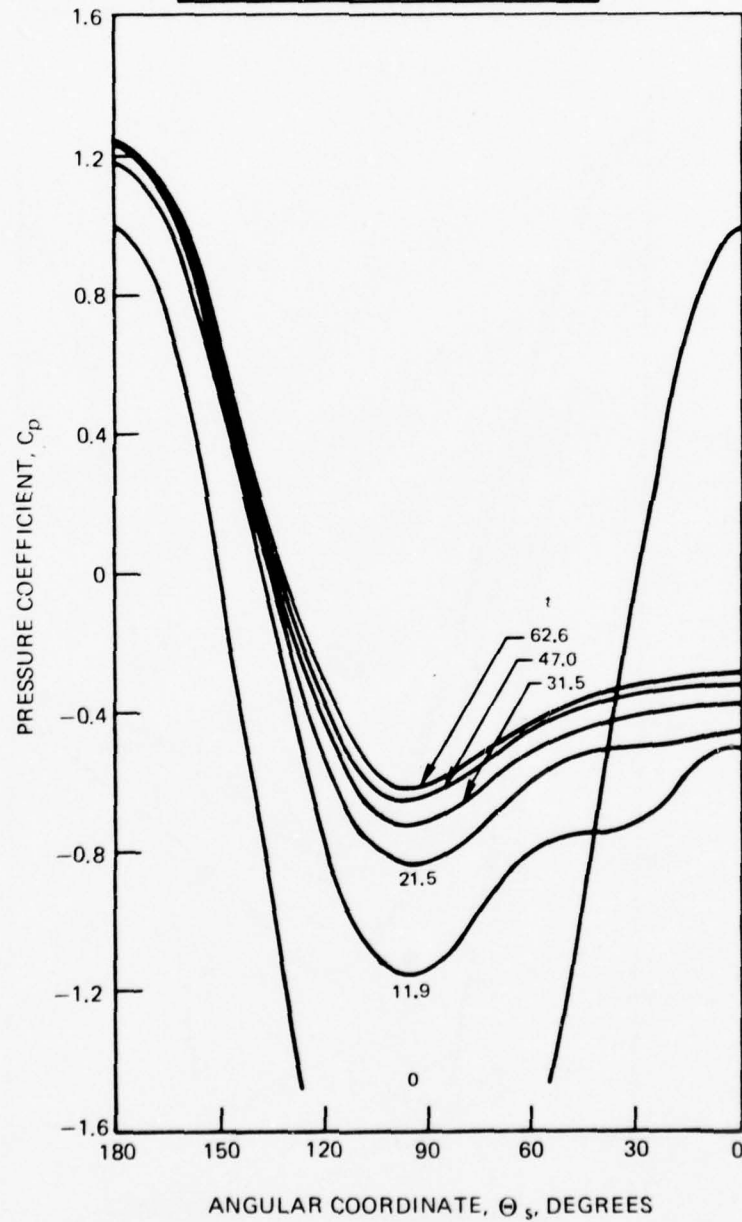
Figure 6—The Development of Surface Pressure with Time for Flow Past a Circular Cylinder at Re = 80
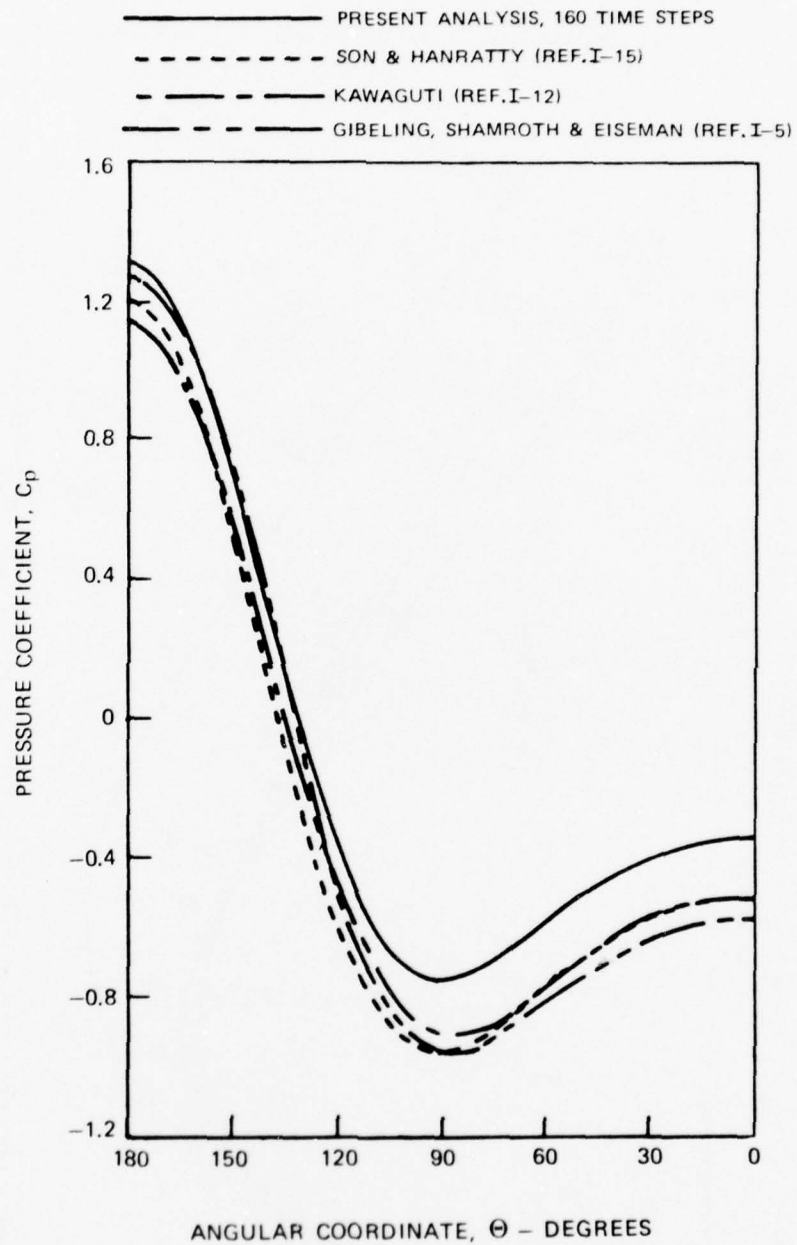
Figure 7—Comparison of Predicted Surface Pressure Coefficients for Flow Past a
Circular Cylinder at Re = 40
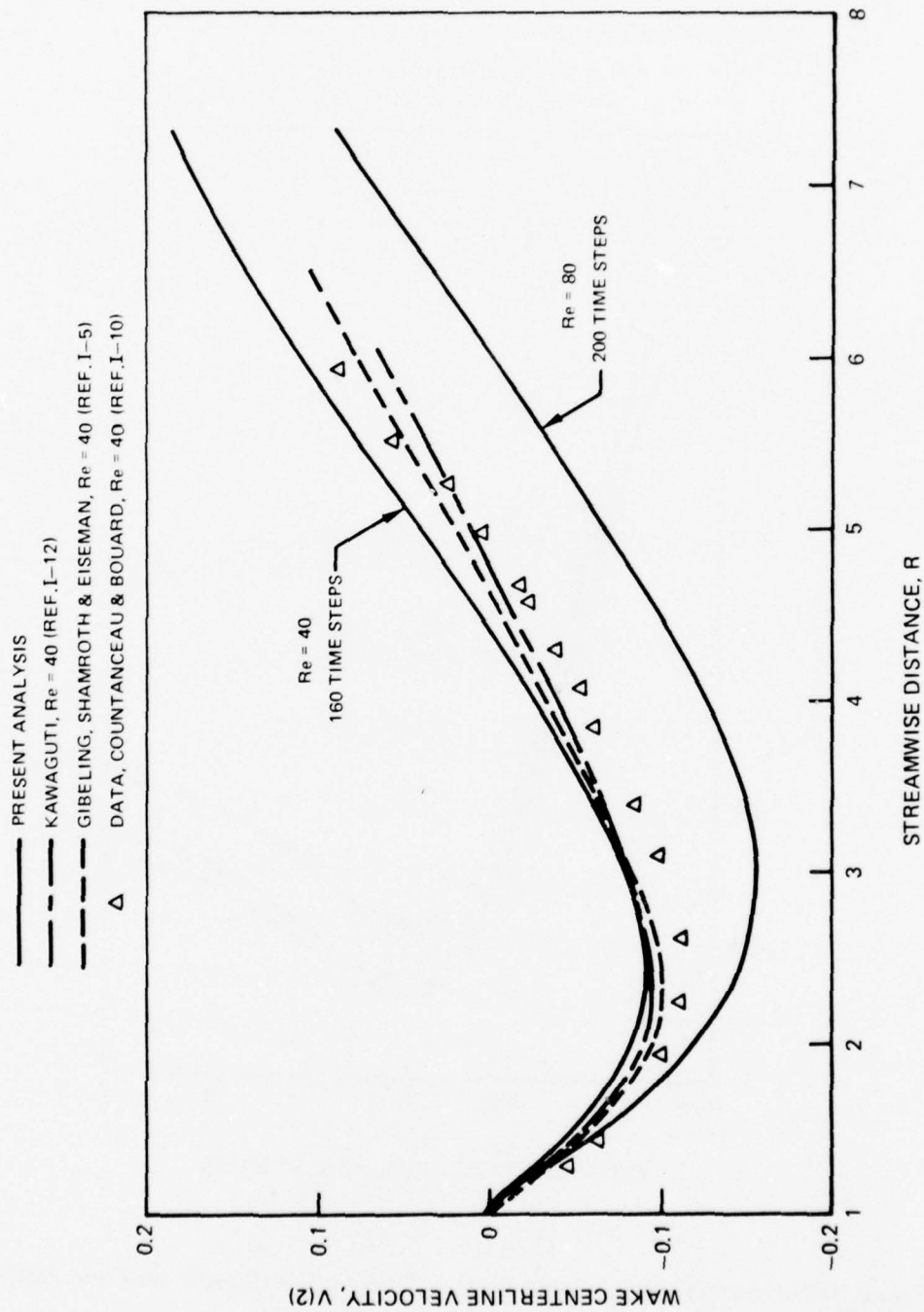
Figure 8—Wake Centerline Velocity Distribution Behind a Circular Cylinder
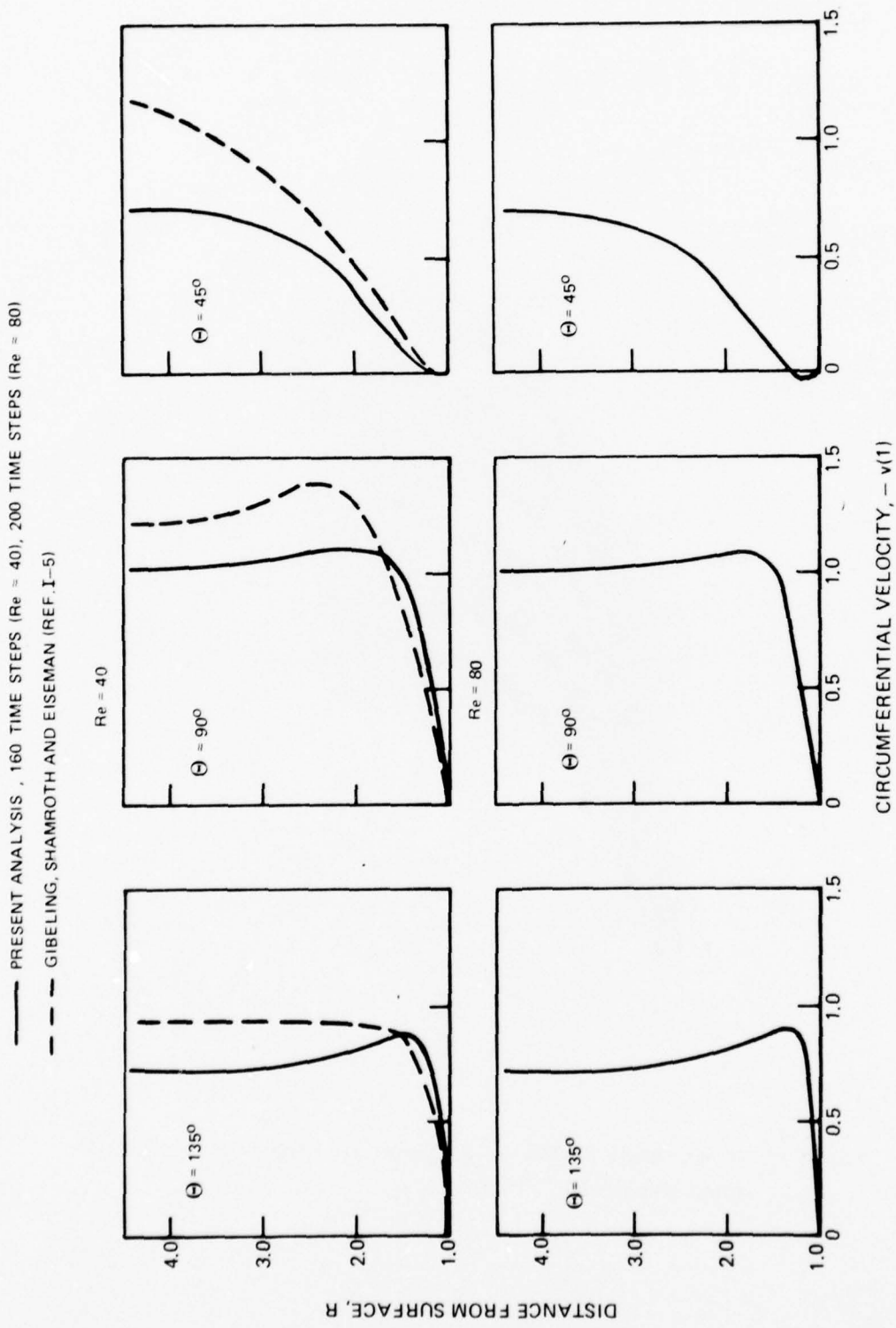
Figure 9—Velocity Profiles for Flow Past a Circular Cylinder

PRESENT ANALYSIS , 160 TIME STEPS (Re = 40), 200 TIME STEPS (Re = 80)

GIBELING, SHAMROTH AND EISEMAN (REF. I—5)

CIRCUMFERENTIAL VELOCITY, — v(1)

DISTANCE FROM SURFACE, R

78—08—189—1
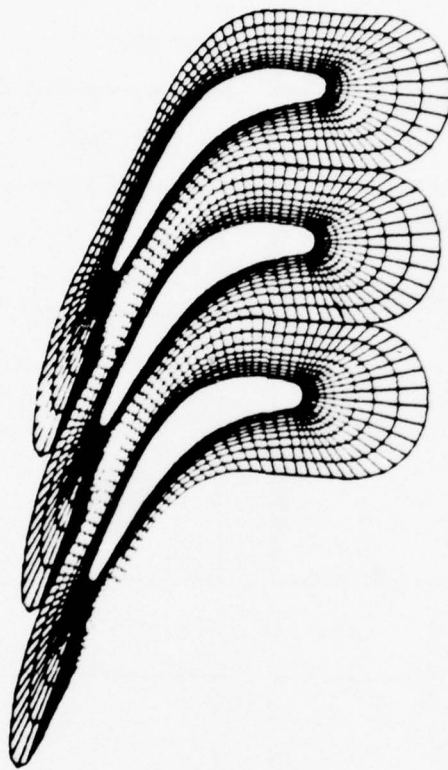
Figure 10—A Coordinate System for a Typical Jet Engine Turbine Cascade
after Eiseman (Ref. I—16)
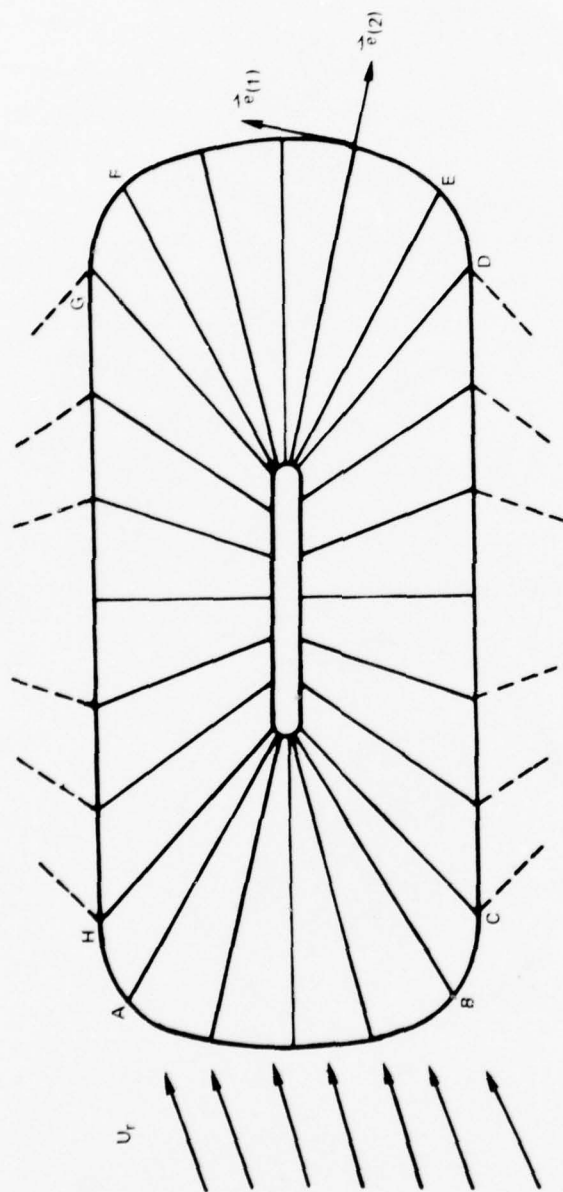
Figure 11—Sketch Used for Illustrating Isolated Airfoil and Cascade Solution Procedures

EXTERNAL INVISCID FLOW

BOUNDARY LAYER

TRAILING EDGE REGION

WAKE
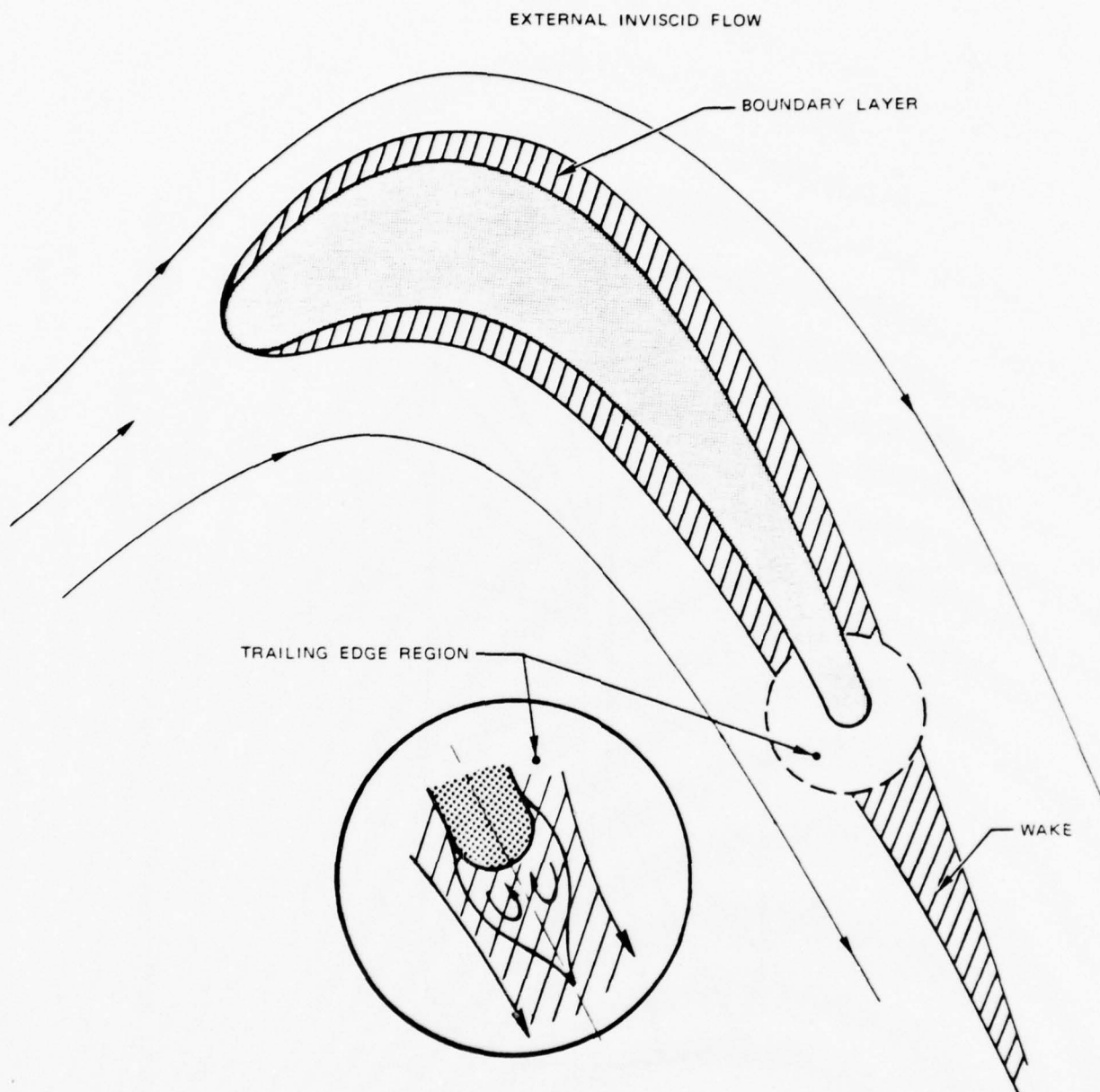
Figure 12   Cascade Flow Field Regions at High Reynolds Number
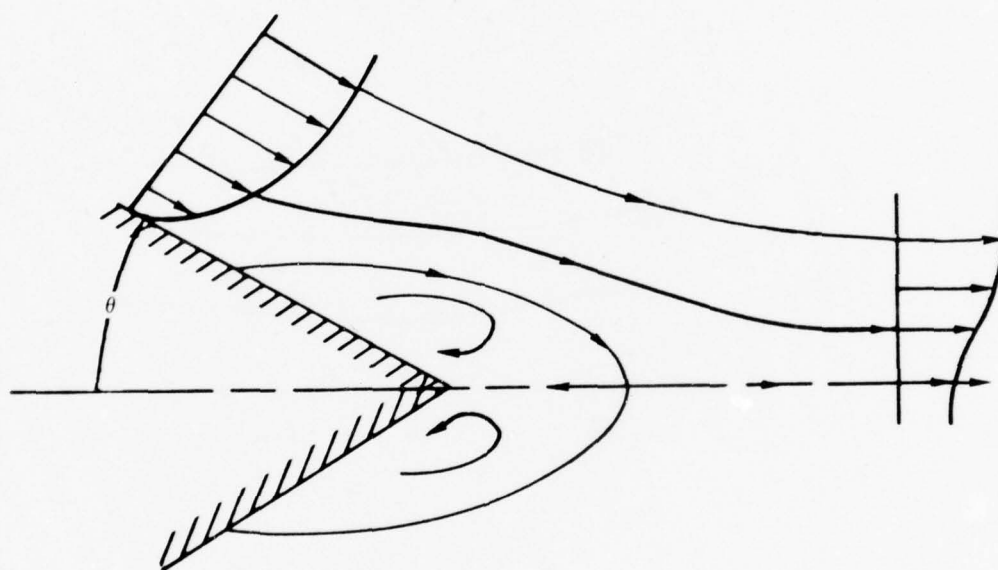
Figure 13   Trailing Edge Region Flow Structure

INVISCID FLOW

δ^*
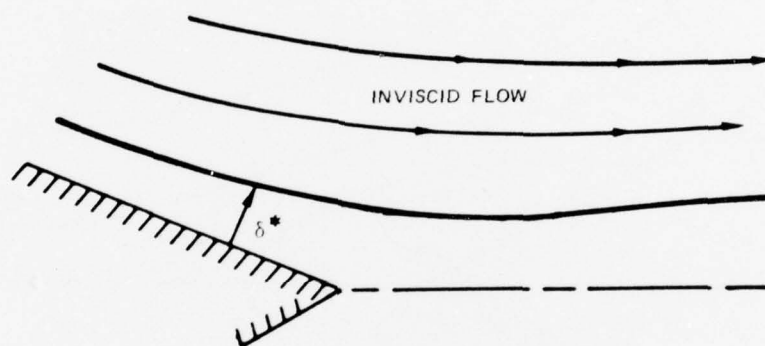
Figure 14   Trailing Edge Region Displacement Surface
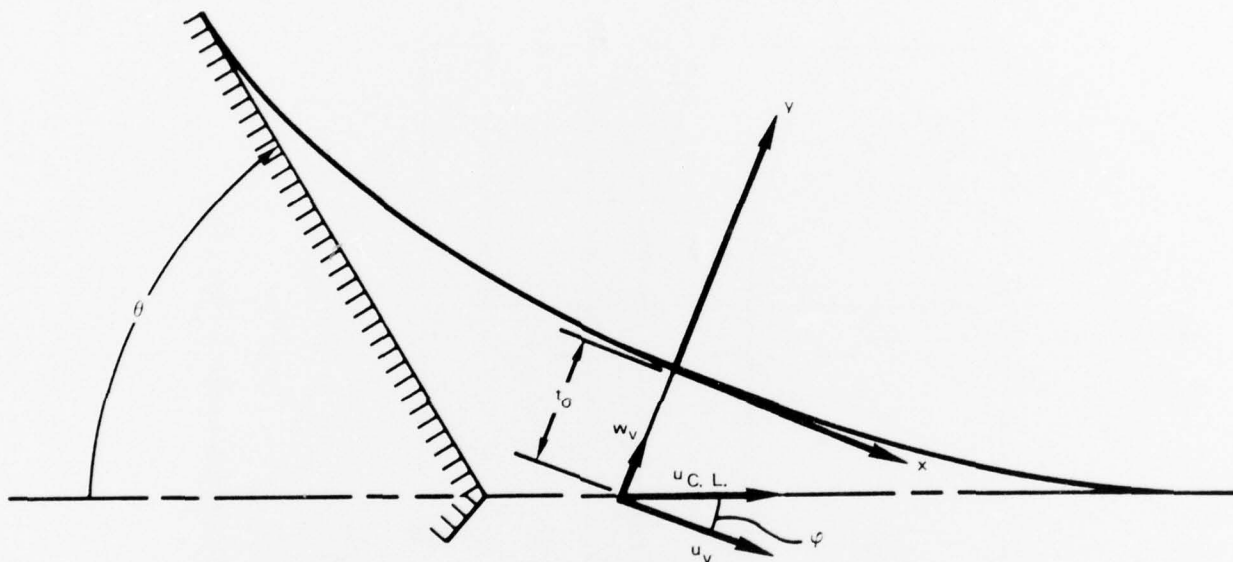
Figure 15   Trailing Edge Region Coordinate Systems

$\epsilon = R_e^{-1/8}$

$a = O(\epsilon^2)$

$O(\epsilon^3)$

$O(\epsilon^5)$

$O(\epsilon^4)$

$O(\epsilon^3)$

$O(1)$
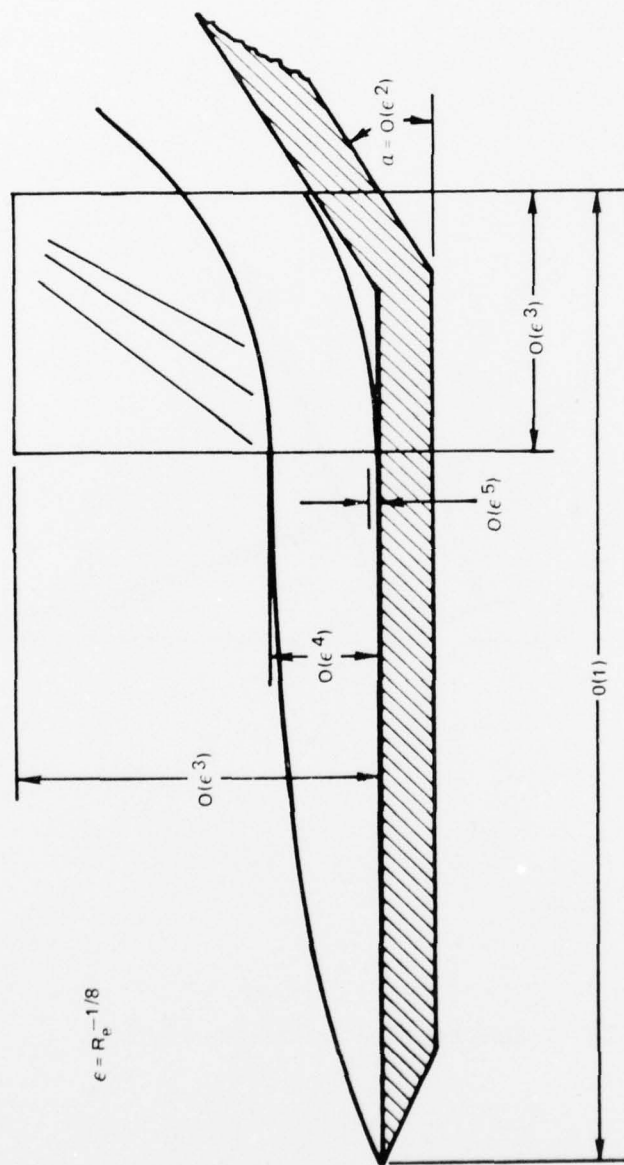
Figure 16   Separation Region Scaling Laws

78-08-97-6
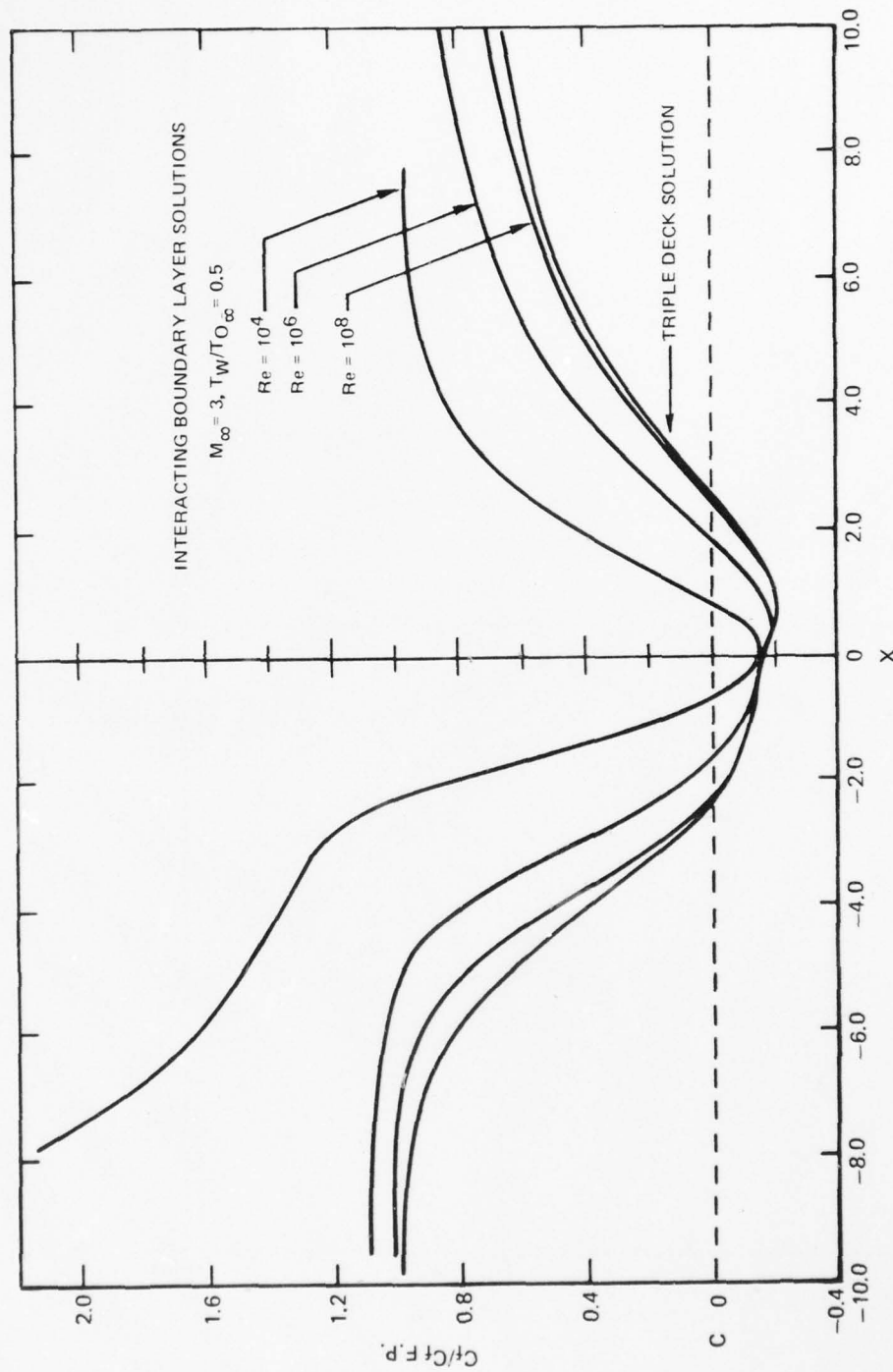
Figure 17 Separation Shear Levels for High Reynolds Number Flows
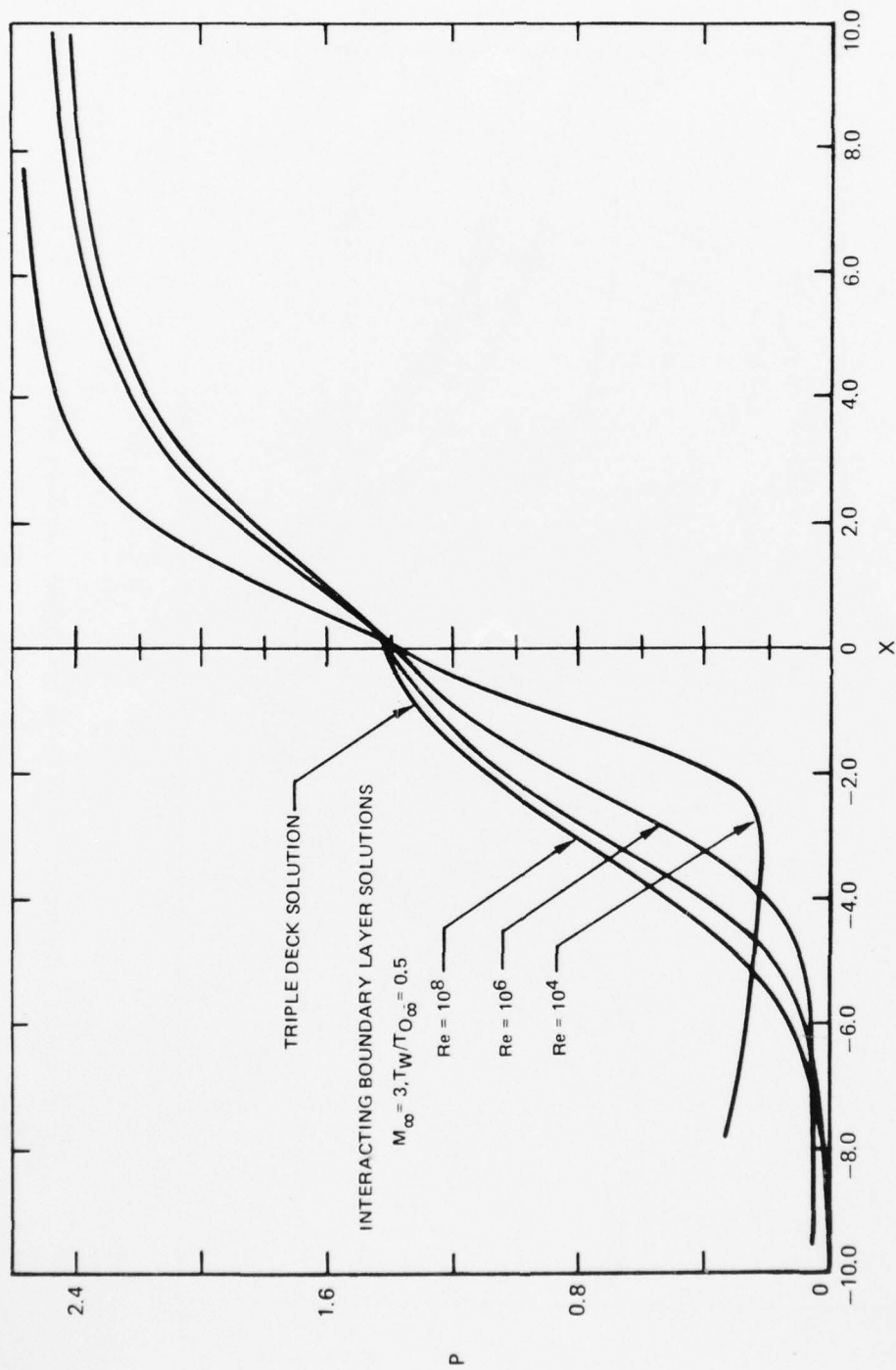
Figure 18   Separation Pressure Levels for High Reynolds Number Flows

M > 1

θ
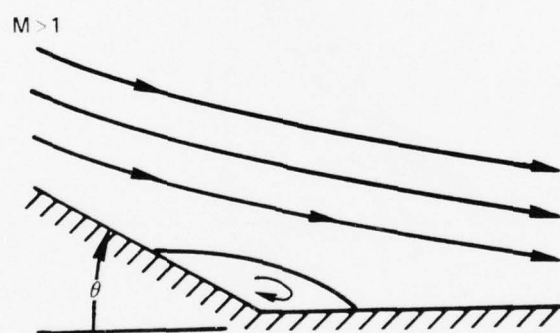
Figure 19   Rotated Compression Corner Flow Field

	SOURCE	ΔY	Y_e	ΔX	REMARKS
	PRESENT	0.25	6.5	0.3	2ND ORDER IN ΔX
	PRESENT	$\begin{Bmatrix} 0.25 \\ 0.50 \end{Bmatrix}$	$\begin{Bmatrix} 6.5 \\ 13.0 \end{Bmatrix}$	0.3	1ST ORDER IN ΔX
	REF II–7	0.6	20.0	0.3	EXTRAPOLATED TO $\Delta X = 0$
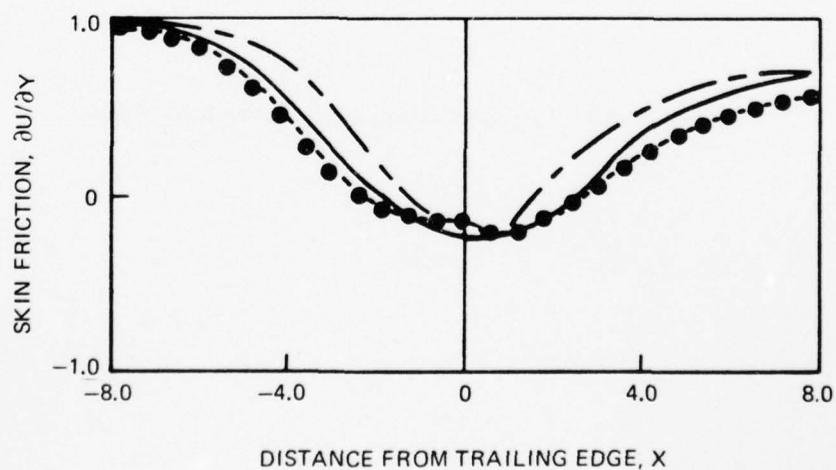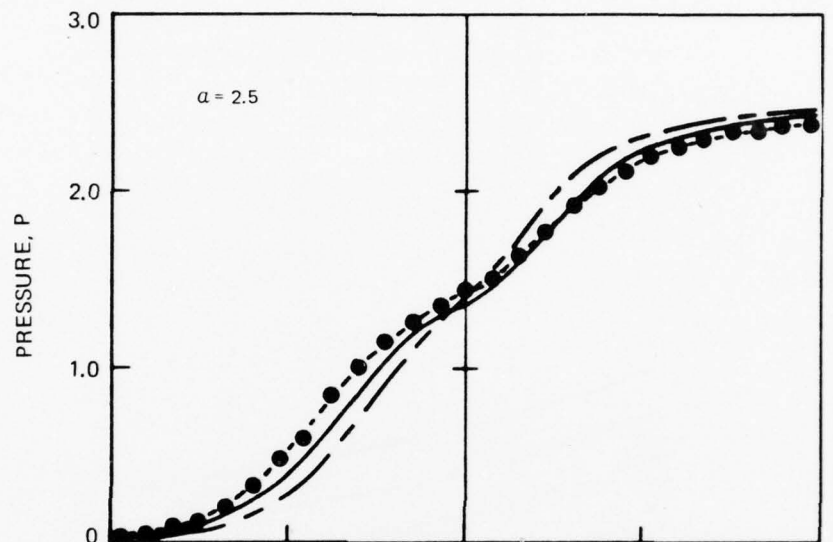
Figure 20   Computer Code Validation for Compression Corner Flow
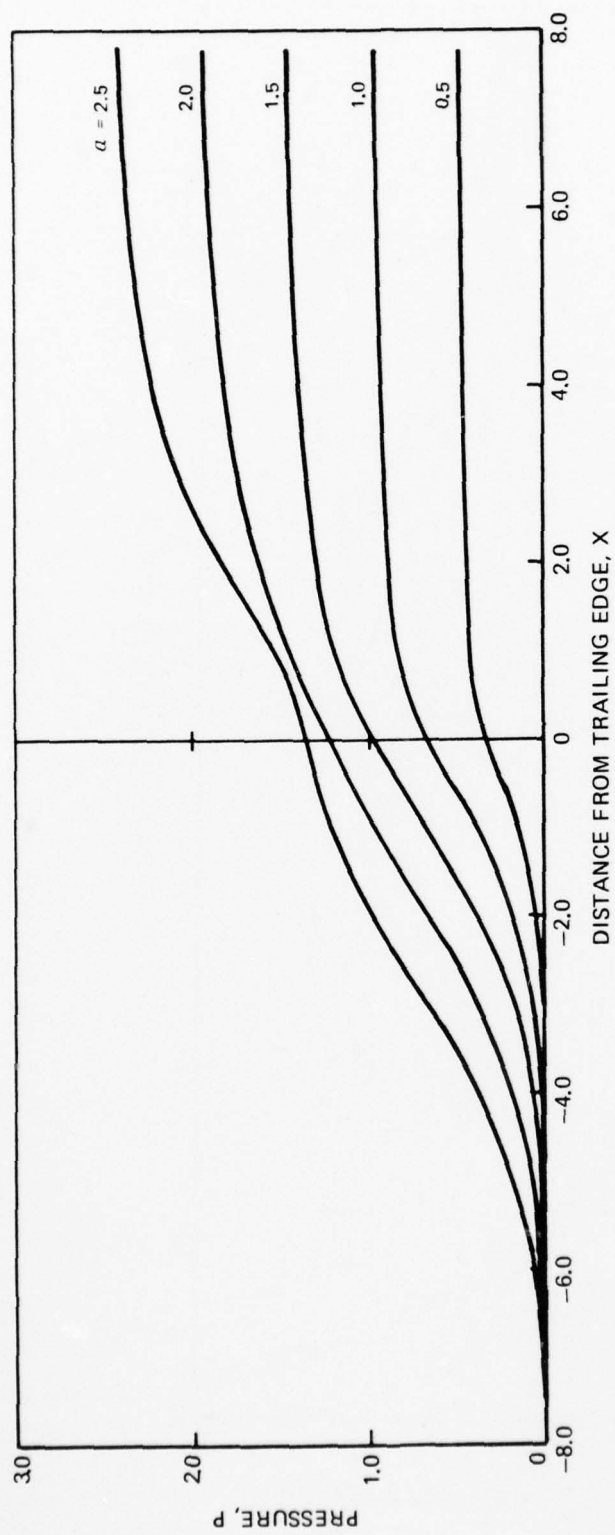
Figure 21   Surface Pressures for Supersonic Compression Ramps

78—08—97—5
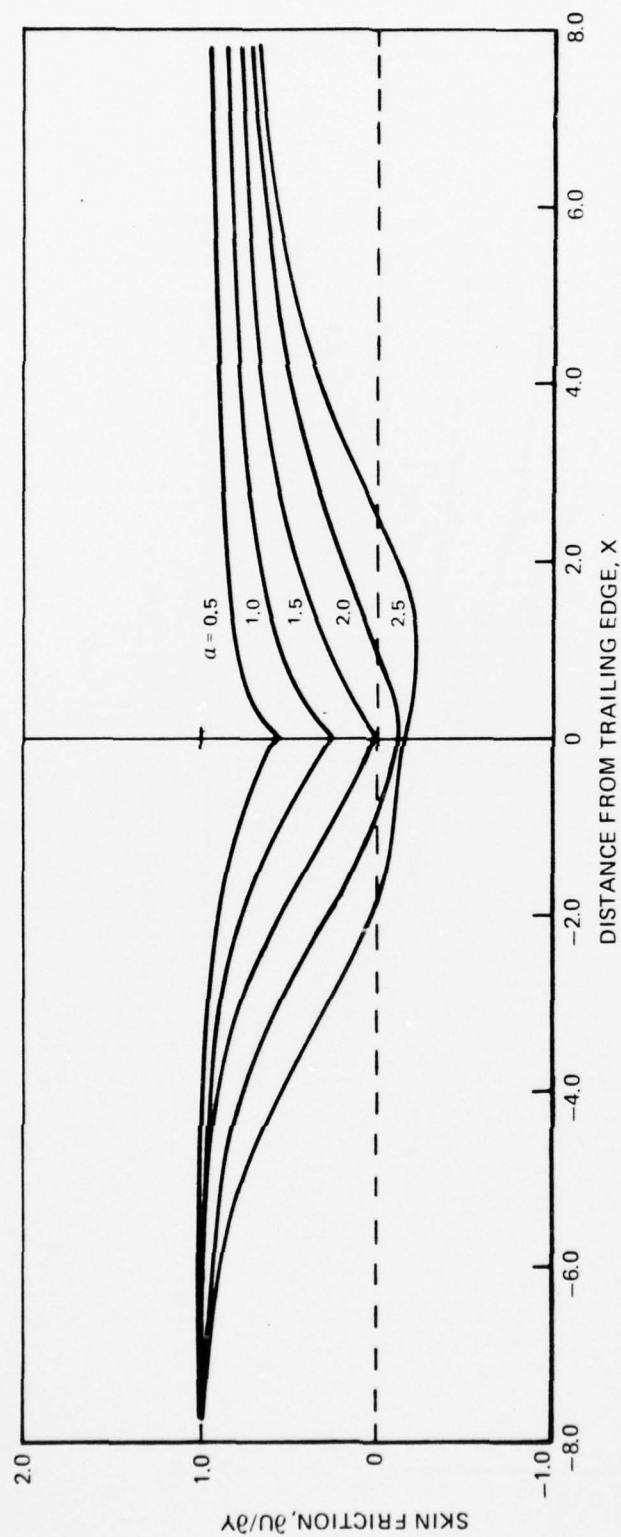
Figure 22 Surface Shear Stress for Supersonic Compression Ramps
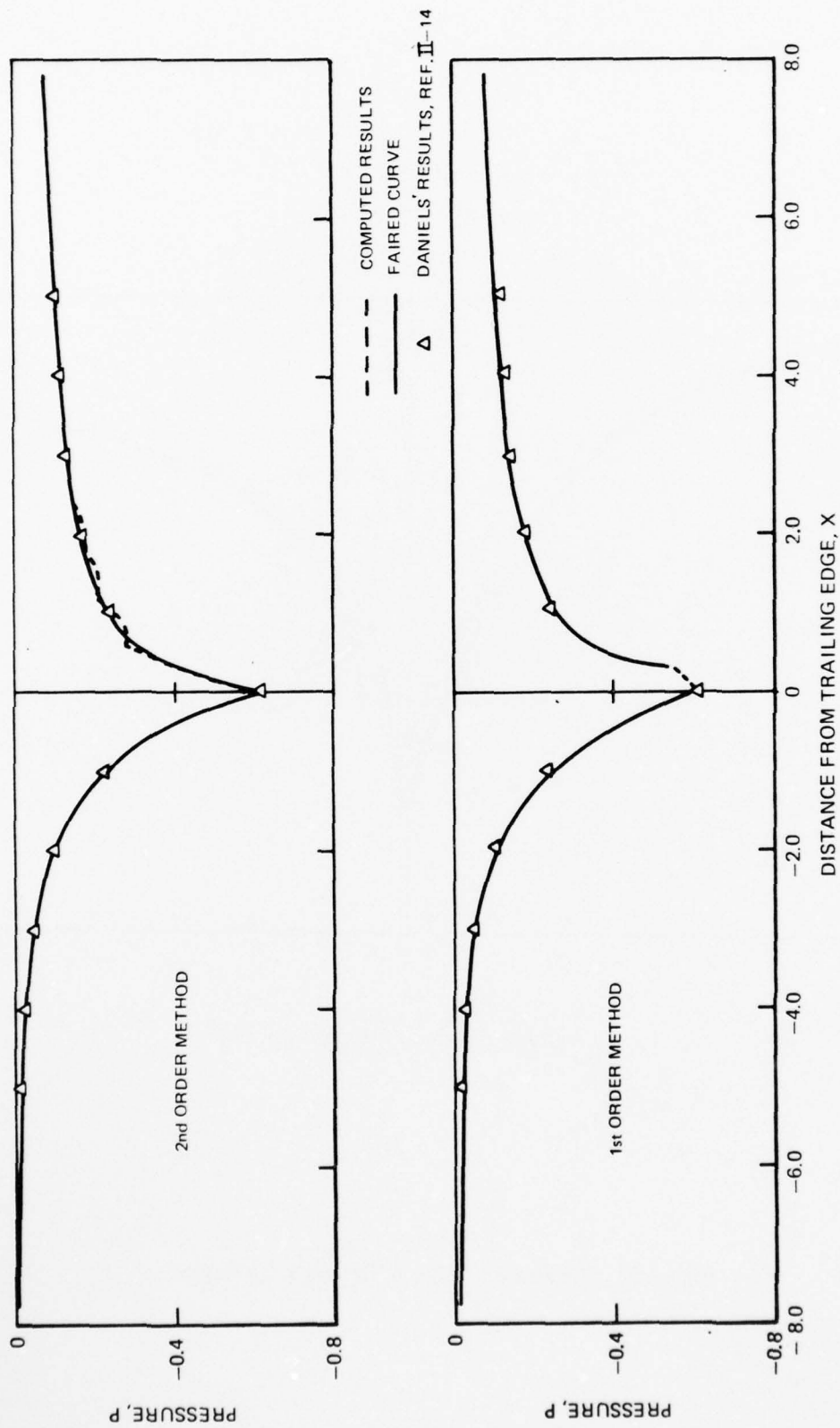
Figure 23   Flat Plate Supersonic Trailing Edge Pressure Comparisons
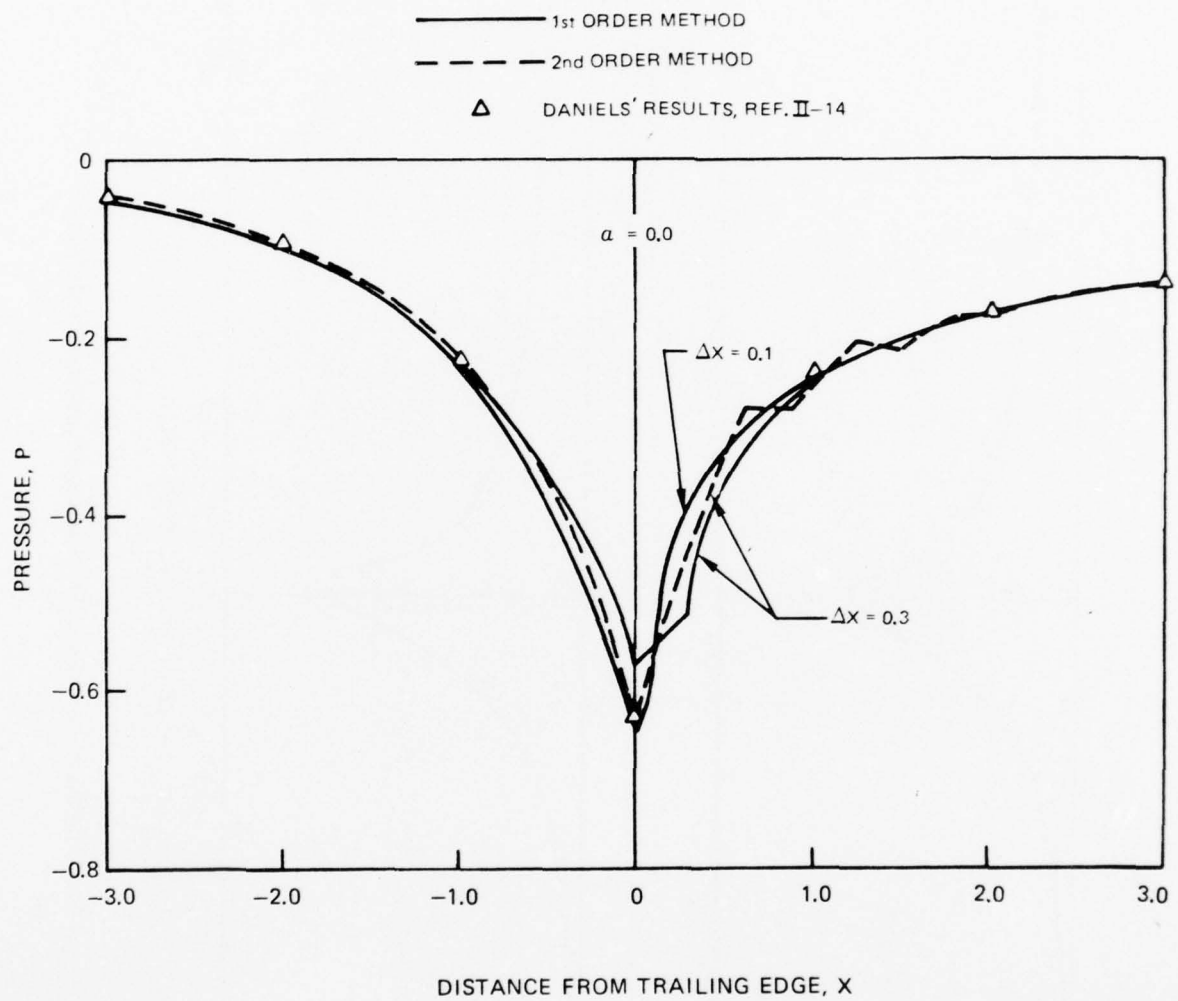
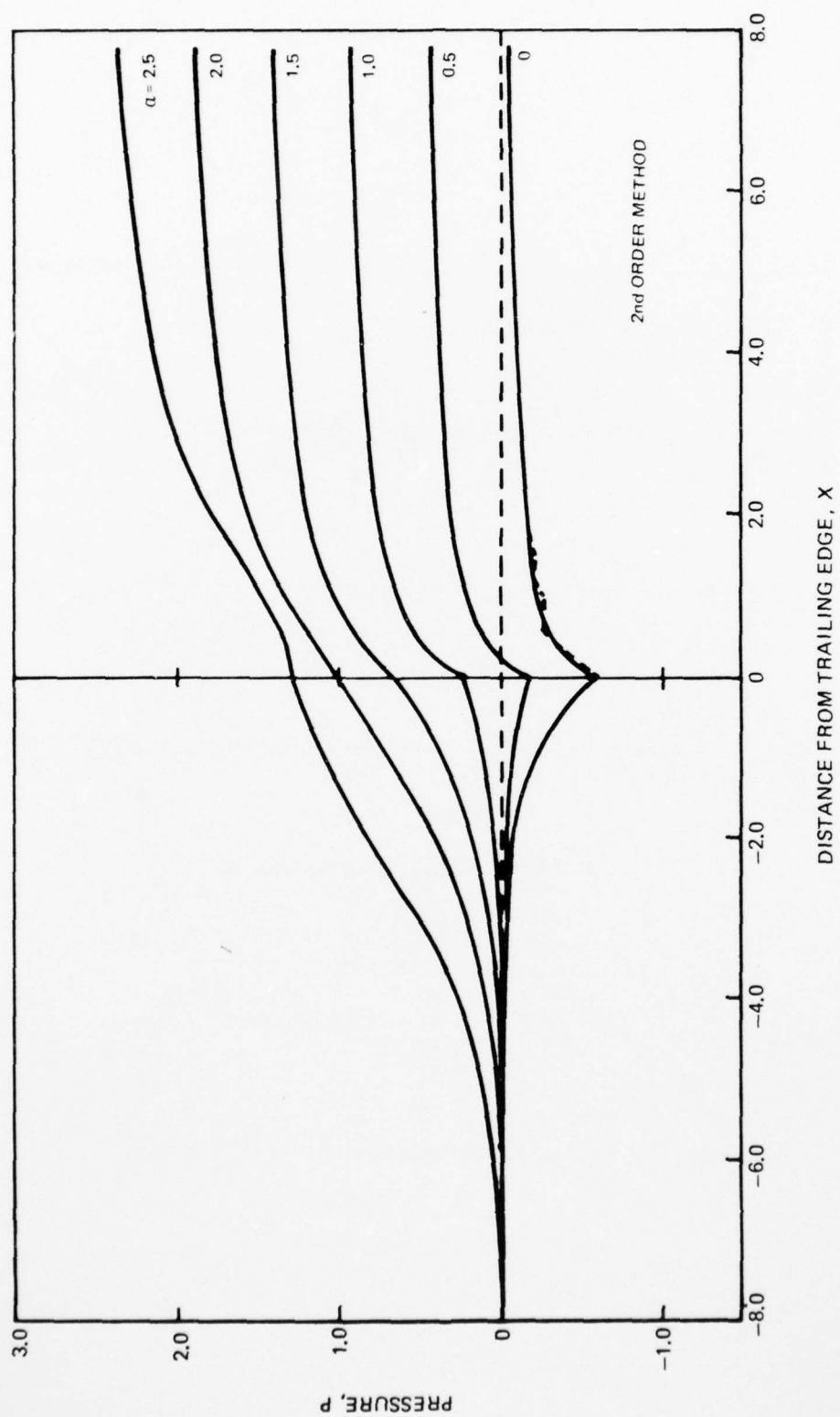Figure 24   Accuracy Details in Trailing Edge Region

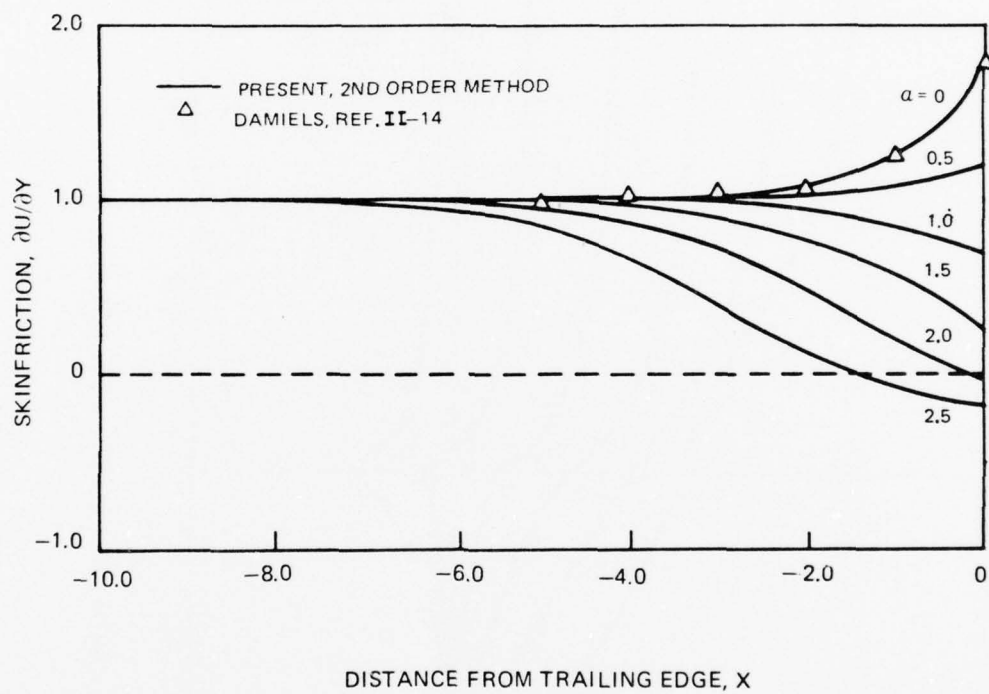Figure 25   Supersonic Trailing Edge Pressure Distributions

78-08-97-3

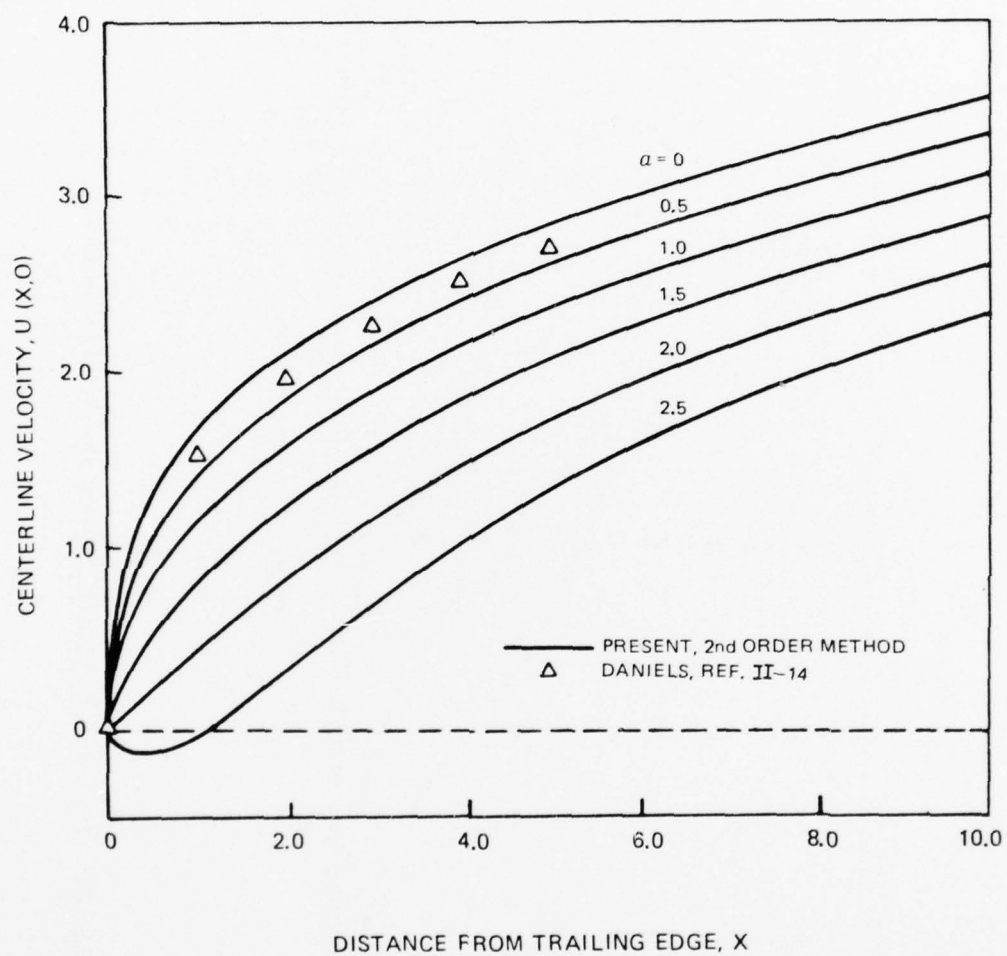Figure 26   Supersonic Trailing Edge Shear Stress Distributions

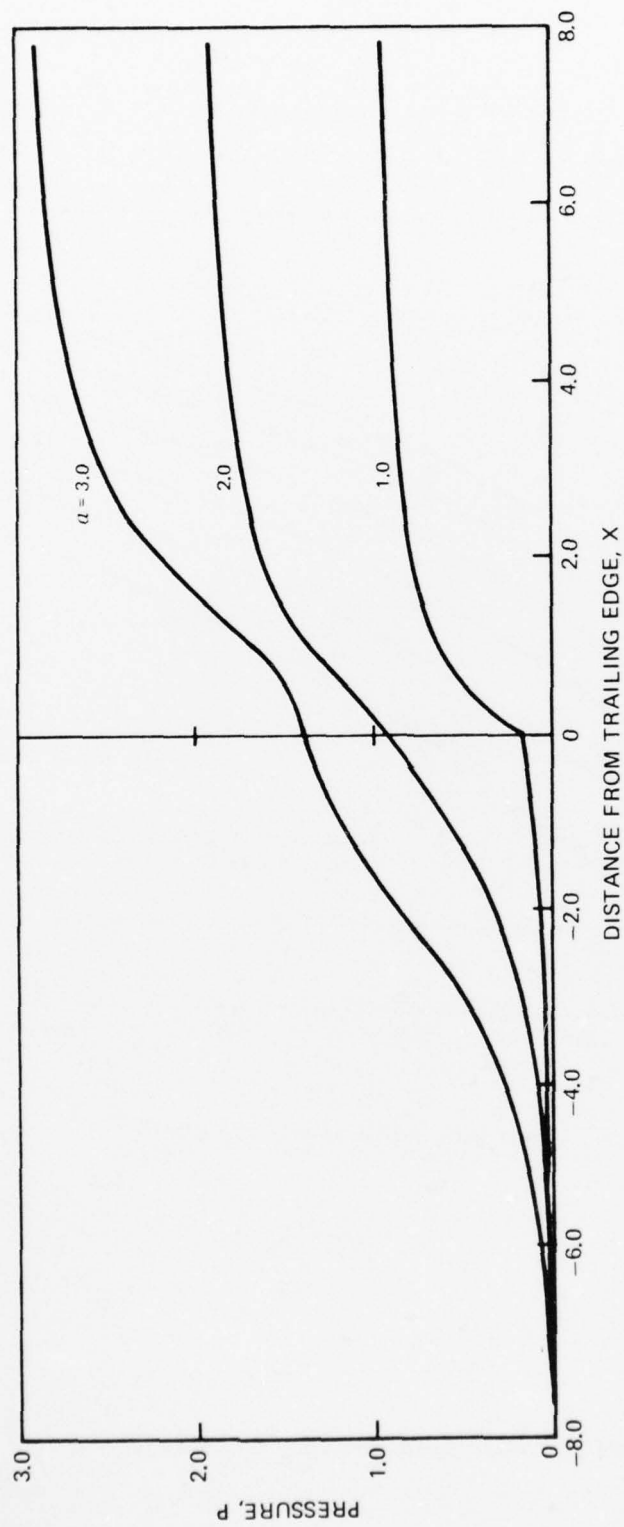Figure 27   Wake Centerline Velocity Distributions

Figure 28   Trailing Edge Pressure Distributions—1st Order Method